Evolution and architecture of an overbank in an ocean-facing canyon-fill.

William J. Taylor[1], David M. Hodgson[1], Jeff Peakall[1], Ian A. Kane[2], Stephen S. Flint[2], Max J. Bouwmeester[2], Josh R. Marsh[2], Euan L. Soutter[2], Ed Keavney, Miquel Poyatos Moré[3], Adam D. McArthur[1], Rufus L. Brunt[2] and Victoria Valdez-Buso[4]

[1]*School of Earth and Environment, University of Leeds, Leeds, LS2 9JT, UK*

[2]*Department of Earth and Environmental Sciences, University of Manchester, Manchester, M13 9PL, UK*

[3]*Departament de Geologia, Universitat Autònoma de Barcelona, Spain*

[4]*Universidade Federal do Paraná, Brazil*

Correspondence: William J. Taylor (*eewjt@leeds.ac.uk*)

Keywords: Canyons, combined flows, confinement, overbank, internal tides, topography, transitional flows

ABSTRACT

Submarine canyon-fills comprise substantial volumes of thin-bedded successions deposited by sediment gravity flows that are either stripped or overspill from adjacent channels into highly confined, topographically complex overbank settings. Here, we document the Punta Baja Formation, a rare example of an exhumed canyon-confined overbank succession with good 3D constraints from the Mesozoic Peninsular Ranges Forearc, Mexico. High-resolution sedimentary logging and drone-captured photogrammetric models reveal that the overbank was a highly dynamic environment, where different bed types point to a variety of flow transformations and complex topographical interactions that evolved through time. The lower overbank is characterised by variable bed thicknesses, grain-sizes and palaeocurrent directions, which point to a wide range of unfiltered flows that overspilled from channels. Thick sandstone beds contain distinct hummock-like bedforms, representing high energy combined flows that repeatedly deflected and reflected against the high relief canyon margin, suggesting complete confinement within the conduit. Locally, thinner beds are disrupted by slides, debrites and scour surfaces on the canyon floor. As the canyon system matured, constituent channels migrated laterally and aggraded. Here, the character of the overbank changes, developing distinct fining- and thinning-upward packages that decay in thickness and grain-size away from the channel axis. Packages are more mud-rich and beds contain mixed grain-size bedforms indicating smaller magnitude, rapidly decelerated transitional flows that failed to interact with the canyon margin. In more quiescent parts of the upper overbank, beds containing rhythmic bundles of silt-rich, mud-draped bedforms are interpreted to be the product of sediments reworked by internal tides. This is the first detailed study of fine-grained fills in an ancient ocean-facing submarine canyon. Canyon-confined overbanks offer a more diverse fill, with flow transformations that demonstrate a complex balance between erosion and deposition, and an absence of discrete internal levée or depositional terrace elements that have been identified in more distal confined overbank settings.

INTRODUCTION

Submarine canyons are narrow, V-shaped valleys incised into lithified rock or sediment that typically occur on upper continental slopes and connect directly to the shelf edge (Daly, 1936; Shepard, 1972; Wynn et al., 2007; Fildani, 2017). They are globally important as conduits that transfer vast amounts of sediment and pollutants from continents to deep-marine basins (Harris et al., 2014; Amaro et al., 2016; Mountjoy et al., 2018; Zhong and Peng, 2021), as efficient sites of organic carbon burial (Masson et al., 2010; Maier et al., 2019), biodiversity hotspots (Cunha et al., 2011; Bianchelli and Danovaro, 2019; De Leo et al., 2020), and dynamic areas of ocean mixing (Allen and Durrieu de Madron, 2009; Zhu et al., 2010; Nazarian et al., 2021). Therefore, it is important to understand the processes that transport, capture and redistribute particulates within submarine canyons, and how they ultimately contribute to the erosion and/or depositional fill over time (Puig et al., 2014).

Sediment and particulates are primarily transported along canyons by sediment gravity flows (SGFs). They are episodic events, driven downslope by the excess density of suspended sediment within the flow (Middleton and Hampton, 1973; Kneller and Buckee, 2000), and can be powerful enough to rapidly modify the seafloor on the scale of metres to tens of metres in a single event (Heezen and Ewing, 1952; Mountjoy et al., 2018; Paull et al., 2018; Talling et al., 2023). Canyon axes are channelised and dominated by sediment bypass and erosion (Kneller, 2003; Stevenson et al., 2015), while their overbank environments within the main canyon confinement surface are sites of deposition (von Rad and Tahir, 1997; Babonneau et al., 2004; Paull et al., 2013; Clift et al., 2014). Consequently, canyon-confined overbank settings are characterised by substantial volumes of thin-bedded sediment gravity flow deposits (Deptuck et al., 2007; Jobe et al., 2015; Maier et al., 2018; Sweet et al., 2019), which offer a more complete record of submarine canyon evolution than their axes.

At present, the flow processes that occur in confined overbank successions are derived from channel-levée systems from mid- to lower slope settings. These models describe deposition by overbanking flows where fully turbulent SGFs are either stripped, or overspill from channels (Piper and Normark, 1983; Hiscott et al., 1997; Peakall et al., 2000), forming discrete end member depositional environments that include flat lying, sheet-like depositional terrace deposits (Hansen et al., 2015; Hansen et al., 2017) and wedge-shaped internal levées (Kane et al., 2009; Kane and Hodgson, 2011; Morris, 2014), which tend to be confined by external levees and some entrenchment into the slope (Kane et al., 2007). However, these models may not represent overbanks in submarine canyons, as canyons are typically more deeply incised into the underlying substrate, and display greater cross-sectional areas and higher axial gradients than channels, with limited development of external levées (Wynn et al., 2007; Hansen et al., 2015).

Studies of modern submarine canyons demonstrate that their overbanks (commonly referred to as terraces) are topographically complex settings with significant erosional and depositional relief, including scours (Paull et al., 2013; Symons et al., 2016; Covault et al., 2017; Li et al., 2020), channel bend cut offs (Fildani and Normark, 2004; Babonneau et al., 2010; Maier et al., 2012), mass transport deposits (Tek et al., 2021; Talling et al., 2022) and sediment waves (Lewis and Pantin, 2002; Wynn et al., 2002; Tubau et al., 2015; Mountjoy et al., 2018). SGFs are particularly sensitive to variations in topography of different scales and orientations (e.g. Baas et al., 2011; Patacci et al., 2015; Soutter et al., 2021), therefore, in topographically complex settings such as canyon-confined overbanks, SGFs may interact with seabed relief and undergo rapid, and significant transformations in rheology and velocity. There is a growing body of evidence for mixed grain-size and hummock-like bedforms, interpreted as the product of flow transformations from initially turbulent unidirectional flows to clay-rich transitional flows, whose depositional style is governed by the balance of cohesive and turbulent forces (Baas et al., 2016; Stevenson et al., 2020; Baas et al., 2021a), and combined flows from interactions with topography (Tinterri, 2011; Bell et al., 2018; Hofstra et al., 2018; Tinterri et al., 2022; Gallicchio et al., 2023). These bedforms impart significant bed-scale heterogeneity within settings previously thought to be homogeneous, and have been documented in lobe off-axis and fringe environments (Baker and Baas, 2020; Privat et al., 2021), channel mouth settings (Brooks et al., 2022) and slope channel-levée systems

(Taylor et al., 2024). These studies show that these bedforms are typically situated close to sites of erosion into mud-rich substrates, abrupt changes in flow confinement and locations with complex seabed topography. Canyon-confined overbank environments should therefore be conducive to flow transformations, but their deposits have not been documented in exhumed canyon-fills, nor are they accounted for in existing depositional models that describe overbanks in confined settings (Kane and Hodgson, 2011; Hansen et al., 2015).

Although SGFs are recognised as the main sediment transport mechanism within submarine canyons, particulates can also be remobilised by internal tides. These currents are tidal frequency gravity waves within a stratified water column generated by surface tidal flows across submarine slopes (Shepard and Marshall, 1969; Shepard, 1976; Gardner, 1989; Garrett and Kunze, 2007). Within the steep walls of canyons, internal tides can become focussed, amplified (van Haren et al., 2022), and strong enough to transport, erode and inhibit deposition of sediment (Petruncio et al., 1998; Hall et al., 2017; Li et al., 2019; Maier et al., 2019). Despite their ubiquity in modern canyons (Wain et al., 2013; Maier et al., 2019; Normandeau et al., 2024), there is a paucity of documented internal tide deposits in ancient deposits (e.g. May and Warme, 2007; He et al., 2011), partly due to an interpretive bias towards SGF deposits in the rock record (Zhenzhong and Eriksson, 1991; Shanmugam, 2003; Dykstra, 2012), or their poor preservation potential, given the erosive power of SGFs within canyon axes that may remove previously deposited layers (Maier et al., 2019; Talling et al., 2023). The overbanks of submarine canyons are therefore postulated to be ideal locations for the preservation of internal tide deposits because they are typically more quiescent environments of deposition, but they have not yet been identified in ancient overbank examples.

To decipher the fine-scale sedimentary record of ancient submarine canyons, exceptional outcrops are required. However, canyons are sites of significant erosion, and although several authors have documented the sedimentology of ancient canyon-fills (Stanley, 1975; Bruhn and Walker, 1995;

Millington and Clark, 1995; Cronin and Kidd, 1998; Satur et al., 2005; Di Celma et al., 2010; Janocko and Basilici, 2021), ocean-facing systems are rarely preserved (Lowe, 1972; Clifton, 1984; Morris and Busby-Spera, 1988; Anderson et al., 2006; May and Warme, 2007; Ito et al., 2014; McArthur and McCaffrey, 2019). Furthermore, due to the poor exposure of fine-grained overbank settings, outcrop studies are often biased towards canyon axes and typically lack three-dimensional control. As such, the stratigraphic evolution of ancient canyon-confined overbank environments remains poorly understood.

This study documents a rare example of an exhumed upper Cretaceous canyon-confined overbank from the Peninsular Ranges forearc basin complex, Baja California, Mexico. The Punta Baja Formation is a well-exposed canyon-fill that faced the Pacific Ocean in the Cretaceous with good 3D constraints. The objectives of this study were to: (i) identify, describe, and interpret deposits that document a variety of submarine canyon flow processes; (ii) detail their stratigraphic and spatial distribution within the overbank fill; and (iii) evaluate the role of complex seabed topography on depositional environments and the spatio-temporal evolution of the Punta Baja canyon-fill. Based on the results, a new sedimentological model for canyon-confined overbanks is presented. This provides an effective tool to aid reconstructions of deep-water processes and environments in preserved sedimentary systems and thereby unlock these cryptic archives as useful indicators of palaeoenvironmental change.

THE PENINSULAR RANGES FOREARC BASIN COMPLEX

The Punta Baja Formation constitutes part of the Mesozoic Peninsular Ranges forearc basin complex (**Figure 1**) that crops out along the Pacific coastal margin of northwestern Baja California and southwestern California (Gastil, 1975; Busby et al., 1998). The stratigraphy of the Peninsular Ranges forearc records the evolution of a long-lived convergent plate boundary from an extensional intra-oceanic arc system in the late Triassic, through a fringing island arc stage during the early- to mid-Cretaceous, to a highly compressional continental arc in the late Cretaceous (Engebretson et al., 1985; Glazner, 1991; Busby et al., 1998).

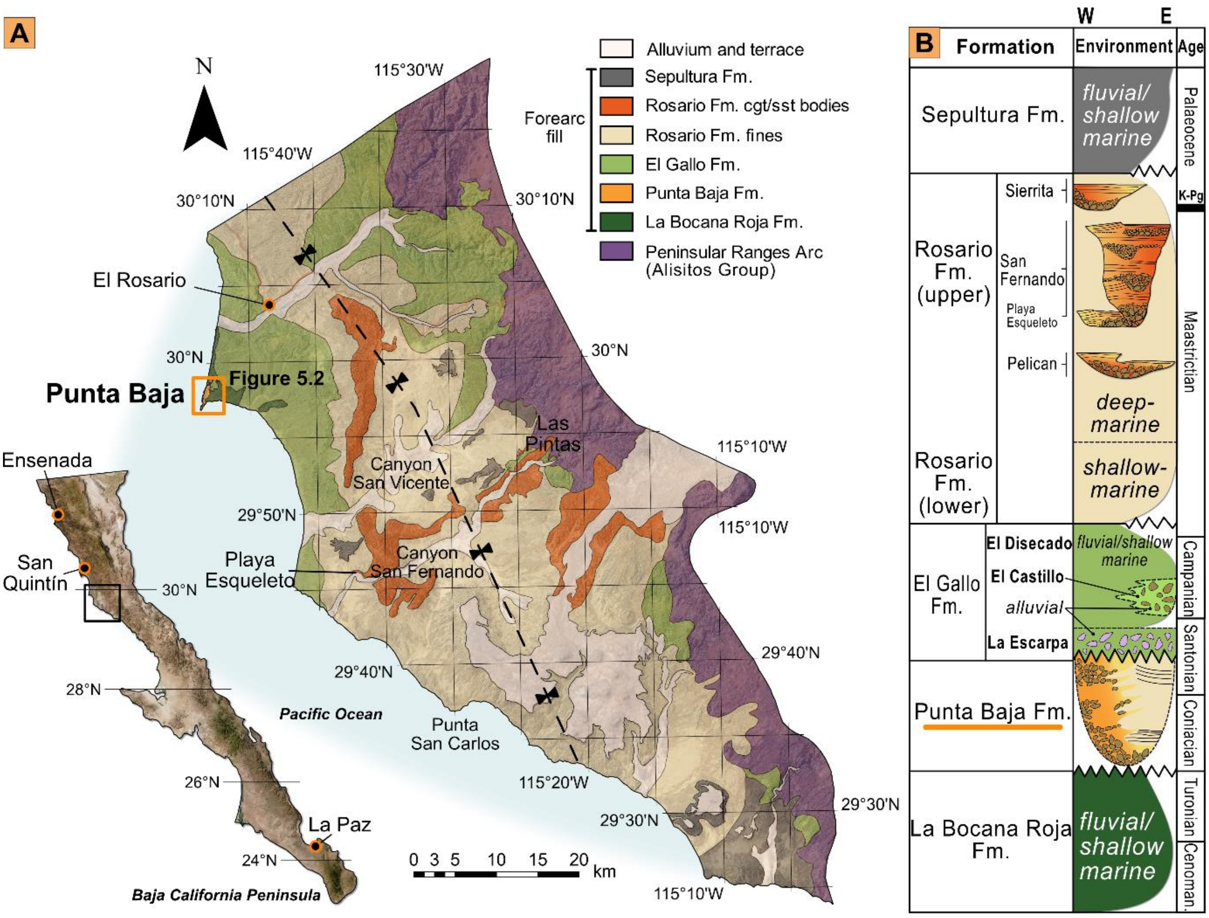

Figure 1. (A) Geological map of part of the Baja California peninsula, showing the main units of the Peninsular Ranges forearc basin complex. Modified from Morris and Busby-Spera (1990) and Kneller et al. (2020). (B) Stratigraphic column showing the main formations and depositional settings of the Peninsular Ranges forearc basin complex.

The latter transition to a compressional stress regime was characterised by reverse faulting and uplift, followed by batholith emplacement and subsequent unroofing. Erosion of the arc basement rocks led to an influx of coarse sediment across a relatively narrow shelf into several ocean-facing forearc basins (Busby et al., 1998; Kimbrough et al., 2001). The orientation and spacing of submarine feeder canyons and slope channel-levée systems was dictated by right-lateral strike-slip deformation from oblique plate convergence (Busby et al., 1998; Kimbrough et al., 2001).

The Peninsular Ranges forearc stratigraphy (**Figure 1B**) comprises: (i) pre-batholithic volcanic and carbonate rocks of the Alisitos Group (Busby, 2004); (ii) post-batholithic non-marine fluvial channel-fills, overbank deposits and palaeosols of the Bocana Roja Formation (Kilmer, 1963); (iii) deep-marine canyon deposits of the Punta Baja Formation (Kilmer, 1963; McGee, 1965; Boehlke and Abbott, 1986); (iv) shallow-marine and fluvial deposits of the El Gallo Formation (Kilmer, 1963; Renne et al., 1991); and (v) shallow- to deep-marine shelf canyon and slope channel-levée complexes of the Rosario Formation (Morris and Busby-Spera, 1988; Morris and Busby-Spera, 1990; Kane et al., 2009; Hansen et al., 2017; Kneller et al., 2020). The vertical alternation of non-marine and deep-marine strata and their unconformable contacts point to alternating periods of uplift, basinward rotation, erosion and subsidence, termed “porpoising” by Busby (2004). By the Palaeocene, contraction of the forearc generated a broad syncline across the axis of the basin complex. This ‘pinned’ the slope at shallow marine depths and led to the deposition of conglomerates and lesser volcanic rocks of the Sepultura Formation (Busby, 2004).

The Punta Baja Formation

The Punta Baja Formation is a well-exposed submarine canyon-fill (Kilmer, 1963; McGee, 1965; Boehlke and Abbott, 1986; Kane et al., 2022), that crops out around the small village of Punta Baja, 12 km south of El Rosario (**Figure 2**). The canyon system likely exploited structural lineaments in the underlying bedrock of the Bocana Roja Formation, which underwent both syn- and post-depositional extensional and contractional deformation during the Cenomanian-Turonian, associated with the releasing and restraining bends of a dextral strike-slip fault zone (Kane et al., 2022). The oblique dextral strike-slip movement likely ceased by the timing of sediment delivery to the canyon (earliest Santonian), as the canyon-fill was largely unaffected by syn-depositional compression (Kane et al., 2022).

The canyon-fill is *ca* 120 m thick and 1.2 km wide and has a relatively wide grain-size range and good 3D constraints, which consist of coarse- and fine-grained domains that represent the canyon axis and overbank environments, respectively (**Figure 3**). The coarse domain comprises conglomeratic channel-fills that record phases of westward lateral migration, characterised by numerous erosion surfaces,

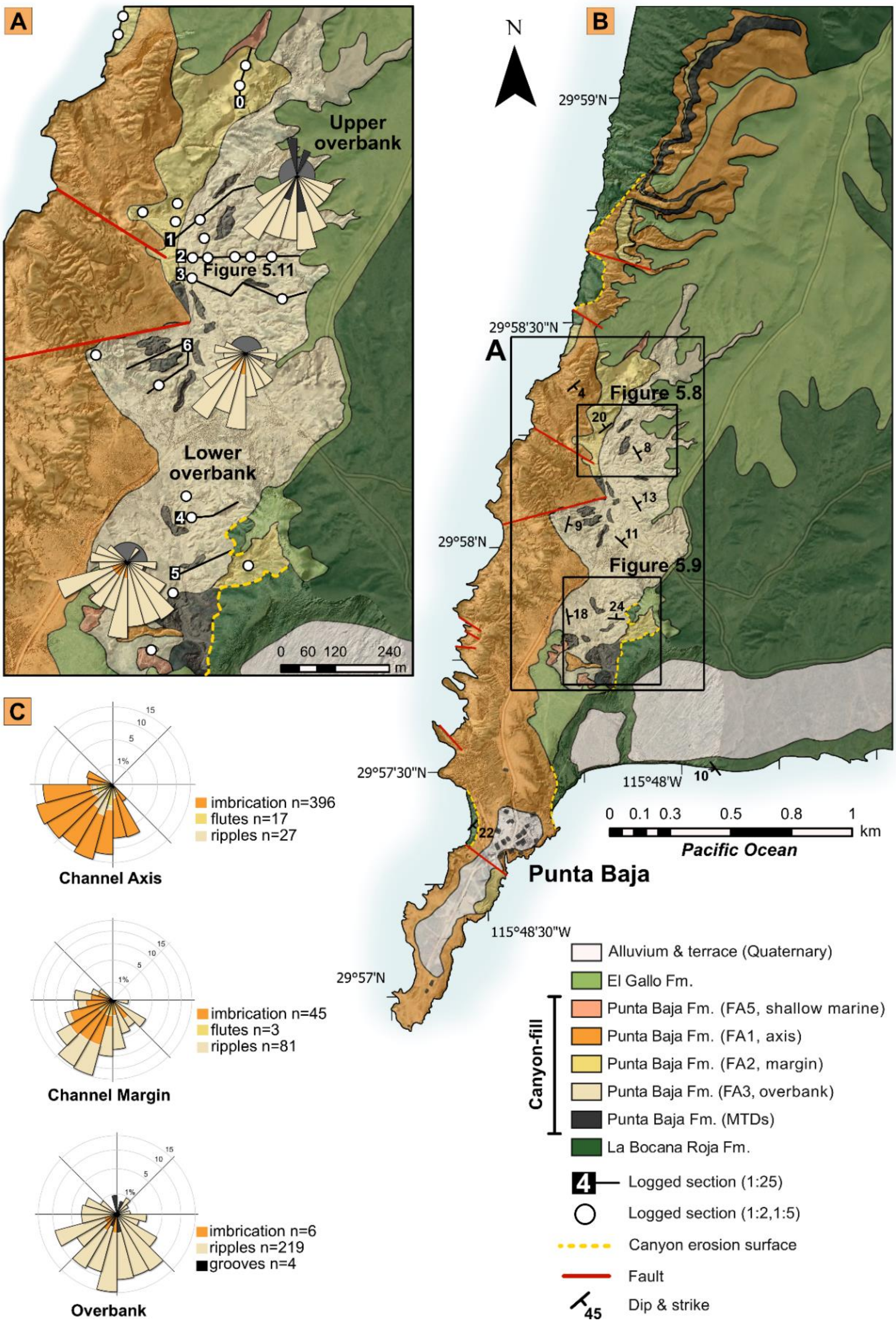

190

Figure 2. (A) Zoomed-in geological map of the Punta Baja overbank (location shown in B). (B) Geological map of the Punta Baja peninsula, with the main formations and facies associations within the Punta Baja Formation overlain onto a drone-captured digital elevation model (DEM). Map location is shown in Figure 5.1. (C) Equal-area rose diagrams showing palaeocurrent directions from conglomerate clast imbrication, flute, groove and ripple foresets for each of the main facies associations.

191

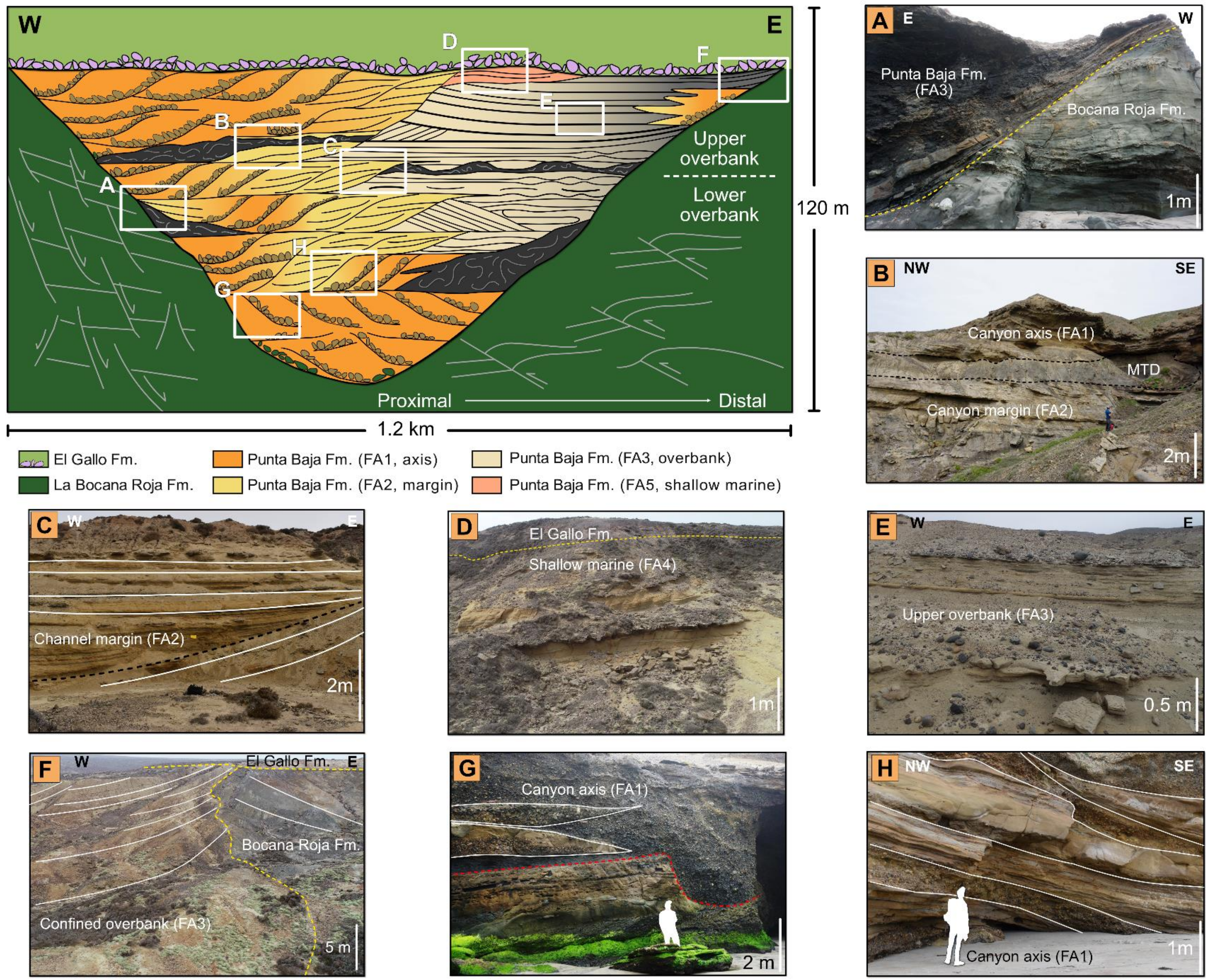

Figure 3. Schematic cross section of the Punta Baja canyon-fill, with photographs highlighting the main facies associations. (A) Overbank packages onlapping onto the Bocana Roja Fm. (B) Canyon axis packages overlying MTDs and channel margin packages. (C) Channel margin packages thinning and onlapping onto steep erosion surfaces. (D) Shallow marine packages truncated by the El Gallo unconformity. (E) Overbank packages within the upper overbank. (F) Overbank packages onlapping onto the Bocana Roja Fm. that are truncated by the overlying El Gallo unconformity. (G) Scour-fill and prominent sandstone bar forms in the canyon axis. (H) Channel margin sandstone packages interbedded with axial conglomerates.

before a subsequent aggradational phase, represented by vertically stacked channel-fills that onlap onto the western margin of the canyon (Boehlke and Abbott, 1986). Towards the east, the channel-fills transition laterally into the fine-grained domain, which comprises a 40 m-thick succession of thin-bedded, heterolithic sandstones and mudstones, interpreted as the overbank (Boehlke and Abbott, 1986), which onlap onto the eastern canyon margin (**Figure 3F**). Regional palaeoflow was to the southwest, and the canyon head was to the northeast, fed by sediment eroded from uplifted plutonic rocks of the Alisitos Group. The overlying El Gallo Formation sits unconformably on top of the Punta Baja Formation, characterised by an angular discordance marked by an extensive transgressive cobble lag deposit which rests on a ravinement surface (Kane et al., 2022).

DATASET AND METHOD

This study focusses on the fine-grained domain of the Punta Baja canyon-fill. The dataset comprises 36 sedimentary logs (301.5 m cumulative thickness), collected across-strike and down-dip, which captured spatial changes in facies and architecture (**Figure 2A**). Logs were collected at 1:25 scale and correlated by walking out distinctive, laterally continuous marker beds. These correlations were aided by interpretations of photogrammetric models captured by Uncrewed Aerial Vehicles (UAV), covering an area of 2.3 km^2. Where the exposure allowed, higher resolution logs, between 1:2 and 1:5 scale, captured measurements of more than 2000 beds. Emphasis was placed on bed-scale changes in thickness, lithology, grain-size, stratal boundaries, constituent bedform types and their dimensions (including bedform amplitude and wavelength). Over 800 palaeocurrent measurements were collected from different parts of the canyon-fill, which recorded clast imbrication, bedform foresets and planforms, flutes, and grooves. These were plotted in equal-area rose diagrams (**Figure 2**). Grain-size was estimated in the field using a hand lens and a grain-size comparator. As clay- and silt-sized grains are difficult to measure accurately in the field, *mud* and *mudstone* are employed as a general term (Winterwerp and van Kesteren, 2004), and to describe argillaceous laminae and bands. The colour of the deposit also gave a useful indication of grain-size, as darker coloured rock typically indicates elevated mud content.

SEDIMENTARY FACIES ASSOCIATIONS AND BED TYPES

The deposits of the Punta Baja canyon-fill were subdivided into four facies associations (**Table 1 & Figure 3**), which comprise FA1 (channel axis), FA2 (channel margin), FA3 (overbank) and FA4 (shallow marine). This study focuses on FA3 which constitutes the canyon overbank setting. Nine bed types were identified, including high-density turbidites (HDT 1 & 2), low-density turbidites (LDT 1 & 2), transitional flow deposits (TFDs 1-3), internal tide deposits (ITDs) and mass transport deposits (MTDs). These bed types have variable occurrence and distribution across the overbank and individual beds can vary spatially in their character. The bed types and their interpreted flow processes are described below, with sketch logs and photographs shown in **Figure 4**. The other facies associations (**Table 1**) provide additional context for the canyon setting; see Bouwmeester et al. (2024) for further detail.

High-density turbidites (HDT 1 and 2)

High-density turbidites (HDTs) are between 15 to 50 cm thick (**Figure 4**). They are coarse to medium-grained, with crude normal grading, erosional lower boundaries (2-10 cm deep) and rare grooves. Locally, they may contain sub-angular mudstone clast intervals or pebble lags. HDT 1 beds are tabular-shaped and comprise a massive sand-rich division at the base of the bed, before passing upward into a sand-rich planar laminated (< 1 cm thick) upper division, with minor wavy and convoluted lamination. HDT 2 beds are similarly characterised by a clean sand-rich basal division and erosional bases, but instead pass into an upper division of sand-rich, dune-scale swale-and hummock-like bedforms (**Figure 5**; amplitude: 10-24 cm, wavelength: 56-80 cm). These form positive relief on bed tops, with clear mounded planform geometries (**Figure 4**). Bioturbation is common in HDTs, with abundant *Ophiomorpha* and *Thalassinoides* traces.

Table 1. Facies associations (FA1- 4), descriptions and environment interpretations. Interpretations here form part of the study by Bouwmeester et al. (2024)

Code	Facies Association	Description	Interpretation	Photo
FA1	Thick-bedded conglomerate and sandstone packages	Highly amalgamated conglomerates (0.5 – 3.5 m thick) and sandstones (0.5 – 2.0 m thick). Conglomerates have strongly imbricated fabrics and are either clast-supported and well-sorted, or matrix-supported and poorly-sorted. They also have steep, erosional basal contacts. Beds are normally-graded with occasional inverse grading. They are sometimes cross-stratified (dune-scale) and contain outsized clasts of the underlying La Bocana Roja Fm. Sandstones (very coarse to medium-grained) are structureless, poorly-sorted, and normally graded, with mud clasts at the bases of beds. Beds are tabular with erosive basal contacts and sharp top surfaces that can contain sporadic pebble cross-stratification. Packages are preferentially stacked towards the western canyon margin.	**Channel axis/submarine braid plain** (Hein and Walker, 1982; Klaucke and Hesse, 1996; Hesse et al., 2001), characterised by bedload deposits indicating scour, bypass and fill from non-cohesive debris flows. Interbedded sandstones and organised conglomerates indicate further deposition and prolonged reworking beneath turbulent high-density sediment gravity flows (Lowe, 1982). Amalgamation suggests multiple stages of scour, bypass and fill as the system migrated laterally and aggraded. Preferential stacking of channel-fills towards the western canyon margin may be in response to dominant extensional faulting and bedrock subsidence on that side, and away from contractional features to the east (Kane et al., 2022).	Figs. 5.3B, G & H
FA2	Medium-to thick bedded sandstone and thin-bedded mudstone packages	Weakly amalgamated sandstone beds (0.5 – 1.5 m thick), often interbedded with silt-rich mudstones (0.1 – 0.3 m thick) and minor conglomerates (< 1 m thick). Sandstones (very coarse- to medium-grained) are moderately- to well-sorted and normally graded. Beds contain mud clasts and flame structures at the base, and sand-rich climbing ripples and planar lamination toward bed tops. Packages typically fine, thin and decrease in dip angle upward and laterally over short distances (<10 m), and onlap onto steep erosion surfaces that truncate other sandstone packages. In some areas packages are deformed, typified by slumped and rotated bedding.	**Channel margin** (Hodgson et al., 2011; Morris, 2014), characterised by rapid suspension settling from fully turbulent, high-density sediment gravity flows with sustained bedload transport (Bouma, 1962; Allen, 1971; Lowe, 1982). Sandstone packages were deposited within the confines of a channel that migrated laterally westwards (Morris, 2014). Flame structures at the bases of sandstone beds are representative of syn- or post-depositional dewatering (Stow and Johansson, 2000). Mud clasts are interpreted as lag deposits, suggesting prolonged erosion (Kneller, 1995). Deformation indicates slumping and remobilisation of soft sediments on unstable channel margins.	Figs. 5.3B & C

FA3	Medium-to thin-bedded, sand- and mud-rich heterolithic packages	Interbedded sandstone beds (0.01 – 0.9 m thick) and faintly laminated mudstone beds (0.01 – 0.7 m thick). Sandstones (very coarse- to very fine-grained) have variable bed characteristics and palaeocurrent directions. Thin-bedded packages comprise normally graded, sharp-based sandstones that contain either asymmetrical sand-rich current ripples, rounded biconvex ripples and mixed grain-size bedforms. Packages also contain rhythmic 'bundles' of mud-draped wavy bedforms, starved laminae and bidirectional flow indicators above sharp-topped turbidite beds. Thin-bedded packages are interrupted by outsized, erosive sandstone beds that contain structureless lower divisions (0.1-0.3 m thick) and planar laminated or hummock-like upper divisions (0.1-0.2 m). Locally, packages are disrupted by MTDs.	**Confined overbank**, characterised by turbidity currents (Bouma, 1962; Mutti, 1992), combined flows (Tinterri, 2011), turbulence-modulated transitional flows (Baas et al., 2009) and internal-tides (Normandeau et al., 2024). HDTs record channel-unconfined flows, and LDTs record flows that were stripped or overspilled from channelised high- to low-magnitude turbidity currents, depositing hummock-like bedforms which indicate flows that deflected off steep canyon walls (Tinterri et al., 2022). TFDs are records of flow transformations from turbulent to laminar across the upper overbank, likely triggered by abrupt changes in flow confinement and/or entrainment of cohesive clay from mud-rich substrates (Baas et al., 2021a). See text for full interpretations.	Fig. 5.3A, E & F
FA4	Medium- to thick-bedded structured sandstones and sand-rich heterolithic packages	Thick-bedded sandstones (0.2 – 1.2 m thick) and thinly interbedded sandstones and mudstones. Sandstones (medium to very fine-grained) are well-sorted and normally graded. Beds contain abundant sand-rich bedforms that resemble hummocky cross-stratification (HCS). *Ophiomorpha and Thalassinoides* traces are common. Palynofacies consist of mixed opaques and amorphous organic matter with poor recovery and poor preservation, and deposits are rich in *Gonylacoid* cysts. Packages typically thicken upward before they are truncated by the overlying ravinement surface of the El Gallo Fm.	**Shallow marine**. Sand-rich HCS is typical of near-shore depositional environments (Harms, 1969). The upward thickening trend might represent progradation of shoreface bars. Ichnofacies and palynofacies assemblages suggest a restricted shallow-marine environment. These packages are interpreted as transgressive deposits, preserved below the wave-ravinement surface of the El Gallo Formation, in the embayment that the Punta Baja canyon likely formed prior to deposition (Bouwmeester et al., 2024).	Fig. 5.3D

Interpretation

HDT beds are interpreted as the deposits of high- to moderate-density turbidity currents. The basal structureless divisions and crude normal grading within beds indicate rapid suspension fallout from a waning, high-density, fully turbulent flow (Kuenen, 1966; Lowe, 1982; Kneller and Branney, 1995; Sumner et al., 2008). The basal surfaces that truncate underlying strata, overlain by mud clast layers and pebble lags also indicate particularly energetic flows that reworked, entrained and bypassed substate prior to deposition (Stevenson et al., 2015). The presence of rare grooves at the base represent bypassing of debritic heads, or potentially previous debris flow events (Peakall et al., 2020; Baas et al., 2021b). The upper planar laminated division in HDT 1 beds likely indicate repeated formation and collapse of near-bed layers termed 'traction carpets', formed under high-concentration flows (Hiscott et al., 1979; Sohn, 1997; Cartigny et al., 2013), which represent decreases in the rate of suspended sediment fallout whilst remaining in the upper-stage flow regime (Allen, 1982; Best and Bridge, 1992). Wavy and convolute lamination may indicate soft-sediment deformation of planar lamination shortly after deposition (Gladstone et al., 2018), or high rates of suspension settling over inactive bedforms forming 'sinusoidal lamination' (Jopling and Walker, 1968; Ashley et al., 1982). HDT 2 beds similarly record deposition under high-density turbidity currents given their basal, sand-rich massive divisions, but with an additional combined flow component (Keavney et al., 2024). In submarine settings, beds with distinct hummock-like bedforms have been interpreted as combined flow deposits from reflection and deflection processes against basin-scale topography (Pickering and Hiscott, 1985; Tinterri, 2011; Bell et al., 2018; Hofstra et al., 2018; Tinterri et al., 2022; Keavney et al., 2024).

Low-density turbidites (LDT 1 and 2)

Low-density turbidites (LDTs) are between 2 to 15 cm thick and comprise normally graded, fine- to very fine-grained sandstone. LDTs have a thin basal structureless sand-rich division with a sharp lower boundary, which passes upwards into a division of sand-rich bedforms (**Figure 4**). LDT 1 bedform divisions comprise low-angle climbing, asymmetric sand-rich current ripples (**Figure 5**; amplitude: 4-

20 mm, wavelength: 40-180 mm), with concave-up or planar foreset laminae with high termination angles (*ca* 40°) against the bases of laminasets. Conversely, LDT 2 bedform divisions are characterised by sand-rich biconvex ripples (**Figure 5**; amplitude: 4-30 mm, wavelength: 80-180 mm), with symmetrical to slightly asymmetrical rounded profiles with a 'pinch and swell' geometry. Biconvex ripples are either low, or high-angle climbing with stoss-side preservation. Internally, foreset laminae are sigmoidal-shaped and drape slightly erosional lower bounding surfaces (1-2 cm deep). LDT 2 beds commonly exhibit a wide range of palaeocurrent directions and reversals in their bedform divisions (**Figure 2A**). Both LDTs have moderate to high bioturbation intensity, with abundant *Scolicia* and *Phycosiphon* traces. LDTs generally fine upward into an upper mudstone division, characterised by subtle siltstone lamination.

Interpretation

LDT beds record deposition from low-density turbidity currents. The thin, structureless basal divisions and normal grading within beds indicate suspended sediment fallout and layer by layer deposition from a waning, dilute turbulent flow (Bouma, 1962; Mutti, 1992; Talling et al., 2012). The overlying sand-rich current ripples indicate deposition under sustained bedload transport (Allen, 1973), and lower rates of suspension settling than HDT beds (Jobe et al., 2012). They also resemble 'sandy current ripples' of Baker and Baas (2020), further suggesting that they formed under fully turbulent conditions. LDT 2 beds record deposition under oscillatory flows, combined with a strong unidirectional component (at 180° to the wave direction). These flows produce the sand-rich biconvex ripples and sigmoidal-shaped foresets through redistribution of sand by vortices on the lee side of the ripple related to the uneven forward and backward strokes of the oscillatory flow components. The top of the lee side of the ripple becomes preferentially 'nourished' by sand, and ultimately generates the rounded, biconvex profile. In submarine settings, these flow components have been attributed to flow interactions with subtle seabed topography (Tinterri, 2011), such as scours or bedform-scale relief (Ge et al., 2017; Hofstra et al., 2018).

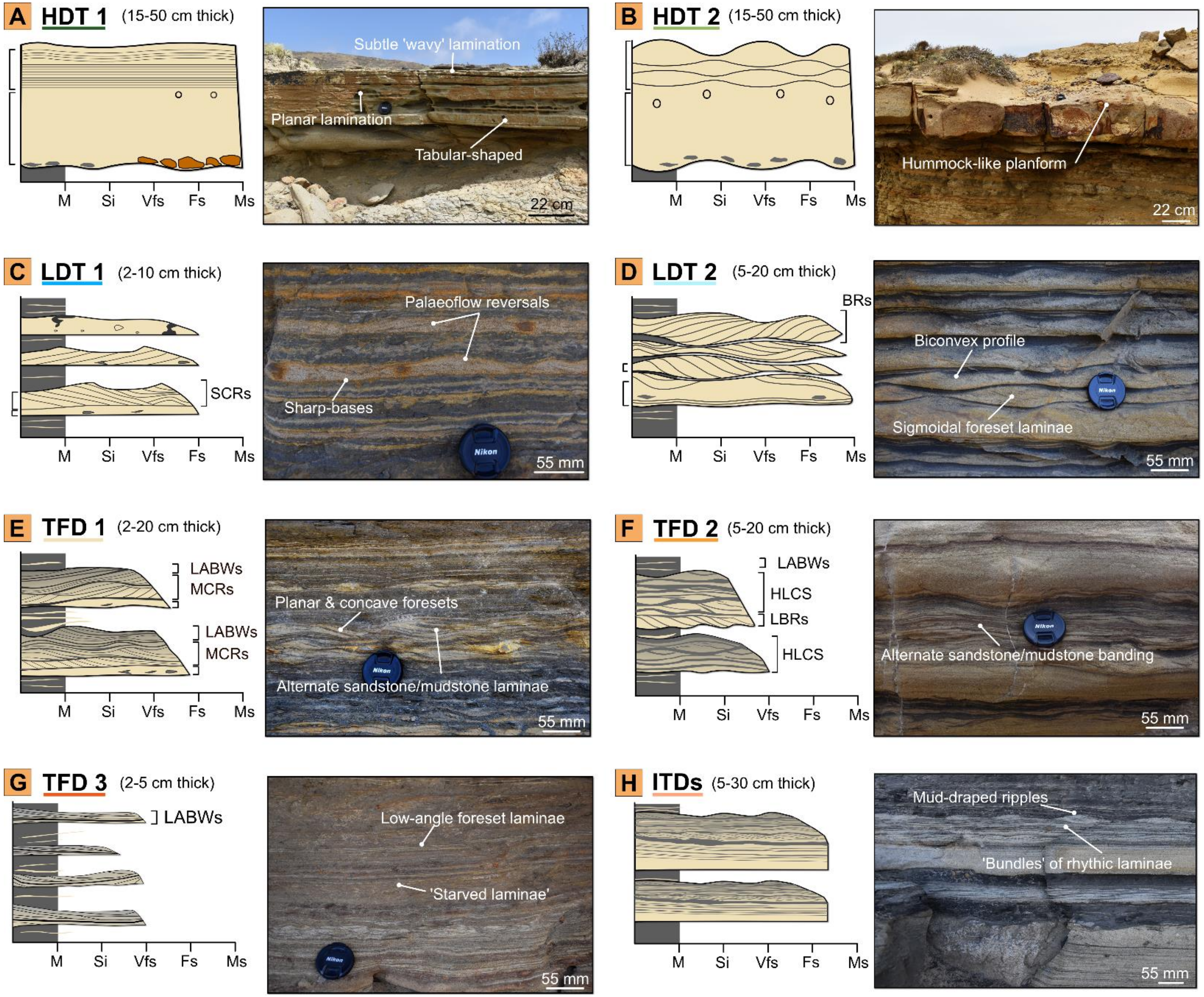

Figure 4. Sketch bed diagrams and representative outcrop photographs which highlight the internal divisions of: (A) HDT 1 beds; (B) HDT 2 beds; (C) LDT 1 beds; (D) LDT 2 beds; (E) TFD 1 beds; (F) TFD 2 beds; (G) TFD 3 beds; and (H) ITDs. HDT, high-density turbidite; LDT, low-density turbidite; TFD, transitional flow deposit; ITD, internal tide deposit; SCRs, sand-rich current ripples; BRs, biconvex ripples; LABWs, low-amplitude bed-waves; MCRs, mud-rich current ripples; LBRs, large biconvex ripples; HLCS, hummock-like cross stratification.

Upper mudstone divisions possibly indicate the distal expression sediment gravity flow deposition, given the presence of subtle siltstone laminae (Boulesteix et al., 2019; 2022).

Transitional flow deposits (TFD 1, 2 and 3)

Transitional flow deposits (TFDs) are defined following Privat et al. (2024), as beds with transitional flow components, but lack debritic components associated with hybrid event beds. Here they are normally graded, fine- to very-fine grained sandstones and siltstones (**Figure 4**). They are distinct in that they contain divisions of mixed grain-size bedforms, which comprise alternations of sand-rich and poorly sorted mud-rich laminae and bands (Chapter 4; Taylor et al., 2024). TFD 1 beds are between 2 to 20 cm thick and have sharp to slightly erosional lower boundaries (**Figure 4**). They typically have a basal structureless, sand-rich division (1-2 cm thick) with sporadic mud clasts, before passing into a division of large, asymmetrical mud-rich current ripples (**Figure 5**; amplitude: 10-60 mm, wavelength: 160-360 mm). Their internal foreset laminae are thin (1-2 mm), concave-shaped, and consist of alternating very fine-grained sandstone and mudstone. The climb angle of constituent laminae progressively increases upwards, which corresponds to increases in bedform wavelength and a reduction in bedform amplitude, before passing into an upper mixed grain-size bedform division of low-amplitude undulating bed waves, herein termed LABWs (**Figure 5**; amplitude: 2-12 mm, wavelength: 200-500 mm). These thin, asymmetrical bedforms contain gently dipping and alternating sandstone-mudstone foreset laminae and bands.

TFD 2 beds are between 5 to 20 cm thick and have slightly erosional lower boundaries (**Figure 4**). They may comprise a structureless ‘dirty’ sand-rich basal division with mud clasts, before passing upward through a division of mixed grain-size bedforms with markedly different geometries than TFD 1 beds. These divisions comprise larger mud-rich biconvex ripples (**Figure 5**; amplitude: 8-40 mm, wavelength: 140-380 mm), with mixed sandstone-mudstone sigmoidal-shaped foreset laminae, and swale- and hummock-like banded sets (HLCS). HLCS banded sets comprise alternating sandstone-mudstone, concave-up and convex-up bands which represent small-scale swale- and hummock-like features, respectively. Internally, bands either drape lower bounding surfaces tangentially at low angles (<10°) or are otherwise fully continuous throughout individual banded sets. Upward transitions between large biconvex ripples and HLCS banded sets are typically gradual and continuous, with only minor erosion observed between some laminae and banded sets. TFD 2 beds typically pass upward into thick, massive mudstone caps.

TFD 3 beds are between 2 to 5 cm thick and are observed isolated in thicker mudstone packages (**Figure 4**). They are sharp-based and comprise very thin, gently dipping sandstone-mudstone laminae and bands. These features resemble LABWs like the upper divisions of TFD 1 beds, but without lower mud-rich current ripple divisions. LABWs typically pass upward into very thin, laterally discontinuous sand-rich laminae that pinch out over 10 cm, forming a streaky texture above the bedform. Most TFD beds fine upwards into an upper mudstone division, characterised by subtle siltstone laminae.

Interpretation

TFDs comprise mixed grain-size bedforms with significant proportions of mud in their laminae and banded sets. Currently, there are two process models that explain the origin of mixed grain-size bedforms in sandstones; episodic near-bed turbulence damping (Lowe and Guy, 2000), or bedform development under mud-laden transitional flows (Baas et al., 2009; 2016; Stevenson et al., 2020). Transitional flow behaviour requires consideration of the balance between flow-velocity controlled turbulent forces and clay-derived cohesive forces (Baas et al., 2009; Sumner et al., 2009). On undergoing deceleration, cohesive clay particles in suspension form flocs and gel due to electrostatic forces between individual particles which act to increase flow yield strength and viscosity, and modulate flow turbulence (Wang and Plate, 1996; Baas and Best, 2002; Haughton et al., 2003; Talling et al., 2004). This initiates a transitional flow, characterised by a laminar plug-flow region with a lack of turbulence, which expands downward from an interval of low flow shear stress, as cohesive forces increase (*sensu* Baas et al., 2009).

TFD 1 beds are therefore interpreted to form under unidirectional transitional flows. The lower division of mud-rich current ripples resemble bedforms deposited under moderately decelerated turbulence-enhanced transitional flow (TETF) and lower transitional plug flow (LTPF) conditions (Baas et al., 2016; Baker and Baas, 2020). Here, a local turbulence enhancement from increased cohesive forces promotes larger bedforms (compared to sand-rich current ripples), before turbulence damping, which results in the gradual increase in bedform wavelength and reduction in bedform amplitude. The upper LABW division indicates deposition under rapidly decelerated upper transitional plug flow (UTPF) conditions (Baas et al., 2016; Baker and Baas, 2020), as further increases in cohesion result in much longer, thinner bedforms (Stevenson et al., 2020). The gradual transition between mud-rich current ripples and LABWs in a single bed suggests progressive flow transformation from turbulent to laminar, as the plug flow region expands downward (Baas et al., 2021a; Taylor et al., 2024). TFD 1 beds are therefore interpreted to form at locations where turbulent flows are forced to decelerate, and/or potentially where flows entrain cohesive mud.

TFD 2 beds record flow transformations under combined transitional flows. Here, flows undergo reflection, deflection and ponding processes with subtle seabed topography as with LDT 2 beds, but instead produce mixed grain-size bedform sequences (Taylor et al., 2024). On interaction with topography, transitional flows take on the dynamics of a combined flow, and deposit and rework sediment into large, mud-rich biconvex ripples (under TETF and LTPF conditions) and HLCS banded sets (under UTPF conditions). TFD 2 beds are therefore indicators of flow transformation from interactions with topography, while undergoing moderate to rapid deceleration over mud-rich substrates.

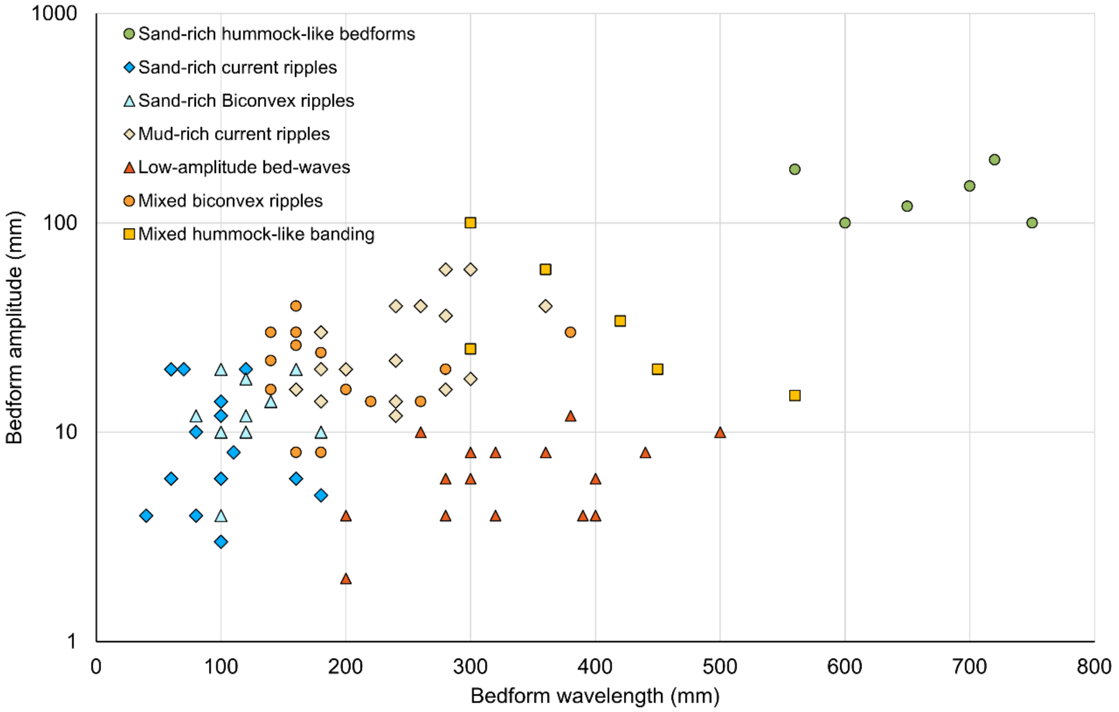

Figure 5. Graph showing the average wavelengths and amplitudes of different bedform types observed within turbulent and transitional flow beds throughout the Punta Baja overbank. Bedform amplitude is plotted with a logarithmic scale.

TFD 3 beds record moderate to rapidly decelerated UTPF and quasi-laminar plug flow (QLPF) conditions. The presence of LABWs and their isolation in thick mud-rich packages supports an interpretation of higher mud content in the decelerating flow, suggesting higher flow viscosity and significant sediment fallout from suspension while maintaining traction (Baker and Baas, 2020; Stevenson et al., 2020). The absence of the lower mud-rich current ripple and sand-rich division found in TFD 1 beds suggests that flows were too highly decelerated and slow moving for LTPF conditions, or that flow transformation was too rapid to produce divisions of mud-rich current ripples.

Internal tide-reworked deposits (ITDs)

ITDs are between 5 to 30 cm thick. They have sharp bases overlain by a basal sand-rich structureless division which passes upward into a planar/wavy laminated and banded division (**Figure 4**). The sand-rich basal division is typically sharp-topped, recording an abrupt change in grain-size. Above this, the deposit is characterised by a division of wavy fine-sand and silt laminae and bands that form distinct sand-mud ‘couplets’. These differ from the banded divisions of TFD beds in that they stack into distinct bundles of thicker sandstone-mudstone bands (> 5 mm) and thinner sandstone-mudstone laminae (1-2 mm). Mud-draped, starved ripples that truncate laminae bundles are also observed. These bear resemblance to mud-rich current ripples as they contain mixed sandstone-mudstone foreset laminae, but they are much smaller in size (amplitude: 6-30 mm, wavelength: 60-140 mm). The starved ripples are draped by mudstone and thin silt-rich laminae. Laterally discontinuous siltstone laminae that pinch out over 1-2 cm are observed at the top of the deposit, before passing into ungraded mudstones (**Figure 4**).

Interpretation

ITDs resemble SGF deposits that have been reworked by internal tides (May and Warme, 2007; He et al., 2011; Maier et al., 2019; Normandeau et al., 2024). The structureless divisions within ITD beds support deposition from waning turbidity currents. However, their sharp tops, grain-size breaks and upper divisions of cyclical laminated and banded bundles (rhythmites) suggest reworking by internal tidal currents (Normandeau et al., 2024). The grain-size breaks at the top of sharp-topped beds might indicate bypass of the fine-grained fraction of a sediment gravity flow downslope (Stevenson et al., 2013), or by internal tides either preventing the fine-grained tail of turbidity currents from settling, or subsequently winnowing the turbidite after deposition (Soutter et al., 2024). The alternation of sand- and mud-rich double laminae in the upper division are interpreted to be records of waxing and waning tidal cycles (Dykstra, 2012), where internal tides resuspend, re-work and deposit sediment across the canyon floor. Similarly, the starved ripples support reworking from a waxing tidal cycle, before the deposition of mud drapes as the cycle wanes (Soutter et al., 2024). The thick-thin cyclicity of couplets is shown to be genetically unique to internal tide deposits (Archer, 1996; Dykstra, 2012), indicating tidally-forced processes, as thicker banded couplets form during stronger spring tides, and thinner laminae couplets during weaker neap tides. Differentiating the deposits of internal tide reworking from the deposits of other deep ocean currents such as transitional flows, is not trivial and requires close examination of sedimentary structures and full consideration of their palaeogeographic context. This is discussed further in the discussion section below.

Mass transport deposits (MTDs)

Mass transport deposits (MTDs) comprise debrites, slumps and slides. Debrites have irregular, erosional lower boundaries, which are overlain by a chaotic distribution of gravel to pebble-sized mud clasts throughout a sandstone-mudstone matrix (**Figure 3B**). They are poorly sorted and lack grading and sedimentary structures. Slumps are characterised by tightly folded, sometimes overturned thin-bedded heterolithic packages, while slides comprise rotated, thin-bedded heterolithic packages which lack internal deformation.

Interpretation

Debrites are deposited *en masse*, under laminar flow conditions by cohesive debris flows (sensu Talling et al., 2012). The irregular, erosive bases suggest high energy scouring and entrainment of underlying substrate which likely created erosional relief on the canyon floor. Slumps and slides likely represent remobilised deposits from failure of stratigraphy which created positive relief (Pickering and Corregidor, 2005).

DEPOSITIONAL STAGES

The thin-bedded heterolithic succession of the canyon overbank (FA3) is subdivided into two distinct depositional stages (Stages 1 and 2 outlined below), which constitute the stratigraphically lower and upper overbank successions, respectively (**Figure 3**). The stages are distinguished based on differences in the proportion and distribution of bed types described above, their sand: mud ratio, variations in bed thicknesses, grain-size, palaeoflow direction and depositional architecture. These are summarised in **Figure 6** and **Table 2**.

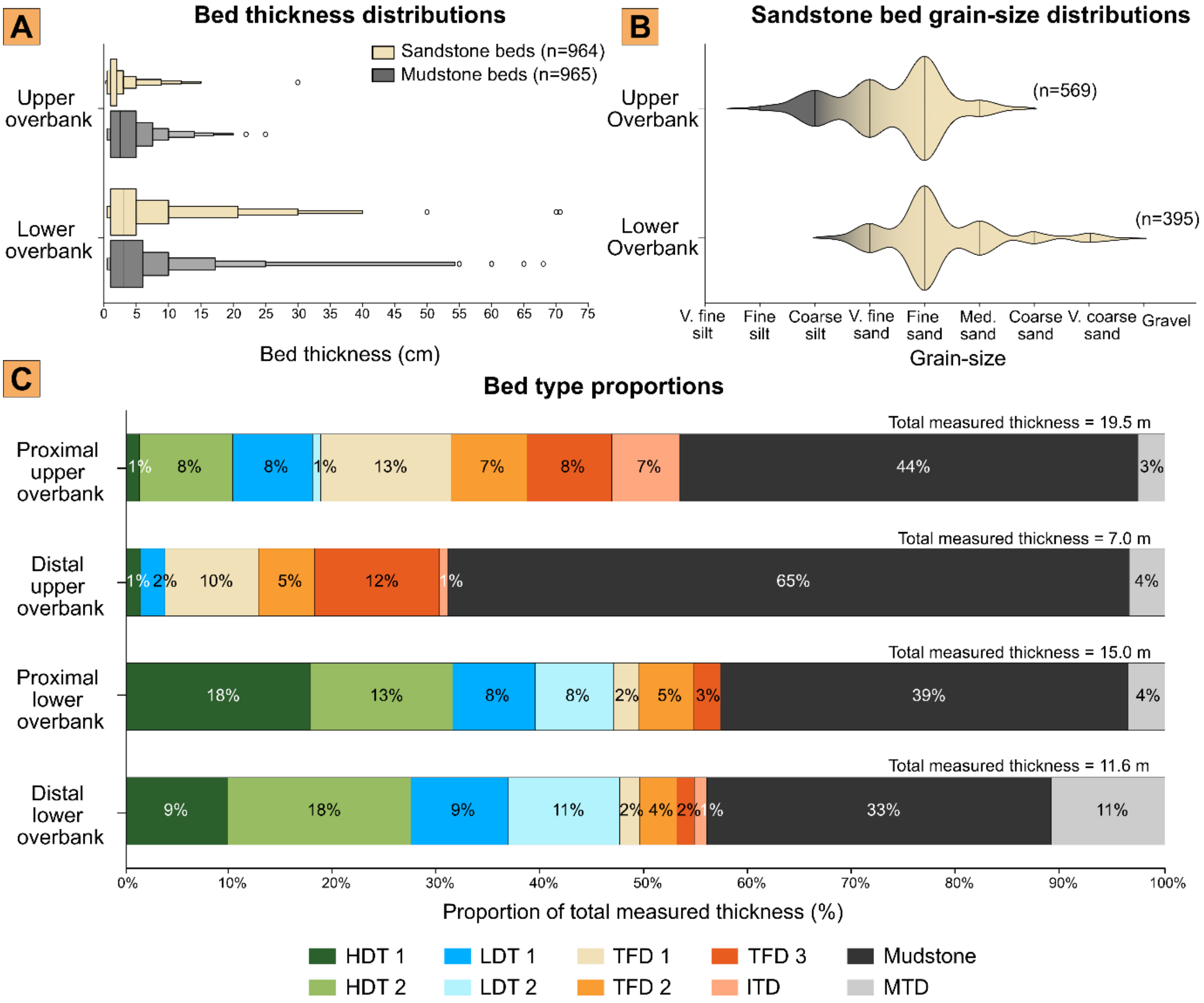

Figure 6. (A) Boxen plot showing the distribution of sandstone and mudstone beds from the upper and lower overbank. (B) Violin plot showing the grain-size distribution of sandstone beds from the upper and lower overbank. (C) Bar plot showing the proportions of the different bed types by total measured stratigraphic thickness of the upper and lower overbank. Proximal refers to locations close to channel-fills, whilst distal refers to locations near the canyon margin. HDT, high-density turbidite; LDT, low-density turbidite; TFD, transitional flow deposit; ITD, internal tide deposit; MTD, mass-transport deposit.

Stage 1 (Lower overbank)

Stage 1 (10-17 m thick) represents the lower overbank (**Figure 3**), and comprises packages of interbedded LDTs, minor TFDs and mudstones, which are interrupted by thicker bedded HDTs (**Figure 7**). Stage 1 packages conformably overlie canyon axis deposits (**Figures 7 & 8**) and contain a significant proportion of sandstone (sand-to-mud ratio of 50:50, **Table 2**), with variable bed thicknesses (0.5-98 cm, **Table 2**) and a wide grain-size distribution (medium silt to gravel), with a tendency toward coarser grain-sizes when compared to Stage 2 (**Figure 6B**). Palaeocurrent directions obtained from ripples are generally towards the south-southeast, though a wide range of directions are observed (**Figure 2**). The proportion of bed types varies little between areas close to channel-fills, and areas close to the canyon margin (**Figure 6C**).

LDT beds comprise ~20% of the total measured thickness of Stage 1 (**Figure 6C**). LDT 1 beds are thin (< 10 cm thick), laterally continuous and evenly distributed across the lower overbank with little lateral variation in sand: mud ratio (**Table 2**). LDT 2 beds are more clustered, forming thicker beds (10-20 cm thick) that thin upwards from the base of the lower overbank, stratigraphically above laterally stacked channel-fills (**Figure 7**). They also cluster near HDT 2 beds and the canyon margin at the eastern edge of the overbank. These beds commonly exhibit a wide range of palaeocurrent directions and reversals within packages close to the canyon wall (**Figure 2A**). TFDs comprise ~10% of the total measured thickness of Stage 1 (**Figure 6C**), TFD 1 and 3 beds are clustered towards the top of Stage 1, while TFD 2 beds are typically clustered near underlying MTDs and scour surfaces (**Figure 7**). ITDs are rarely observed in the lower stage of the overbank.

HDTs comprise ~29% of the total measured thickness of Stage 1. They form discrete, outsized beds that are either laterally continuous for hundreds of metres with only minor changes in bed thickness (**Figure 8**), or otherwise form isolated, highly bioturbated lenses which pinch out laterally over tens of metres (**Figure 9**). HDT 1 beds are common near adjacent channel margin deposits on the western side of the lower overbank, where they are typically tabular-shaped with strongly erosional bases and pebble lags (**Figure 8**). With lateral distance from channel-fills, they gradually change character, becoming less erosional to eventually resemble hummock-like HDT 2 beds at locations within 10-20 metres of the canyon margin (**Figure 9**). HDT beds generally pinch out abruptly at the canyon margin boundary.

Locally, thinner bedded packages in-between HDT beds are disrupted by MTDs (~11% of the total measured thickness of Stage 1). These mostly occur as mud-rich debrites, which are 4 to 5 metres thick near canyon margins (**Figure 9**), but thin to form discontinuous lenses across the overbank. Debrites

Table 2. Thickness, number of beds measured, sandstone bed thickness average, range and standard deviation and sand: mud ratio from proximal and distal areas of the overbank depositional stages. Data is compiled from 2,027 beds measured across the Punta Baja overbank (FA3).

Depositional Stage	Proximal/distal to channel-fills	Thickness	No. of beds measured (sandstone beds)	Average, range and standard deviation of sandstone bed thickness	Average sand: mud ratio
Stage 1: Lower Overbank	Proximal	10 m	590 (296)	Average = 5.7 cm Range = 0.5-98 cm StDev. = 12 cm	50:50
	Distal	7 m	297 (148)	Average = 8.1 cm Range = 1-50 cm StDev. = 9.6 cm	50:50
Stage 2: Upper Overbank	Proximal	28 m	901 (449)	Average = 2.6 cm Range = 0.2-30 cm StDev. = 5.1 cm	41:59
	Distal	12 m	239 (120)	Average = 1.6 cm Range = 0.1-15 cm StDev. = 2.5 cm	30:70

are observed either near slumped packages of tightly folded, occasionally overturned LDT beds near the canyon margin (**Figure 7D**), or otherwise underlie laterally discontinuous, wedge-shaped HDT beds (**Figure 7C**). Slides are common at locations close to channel-fills and comprise rotated packages of LDT beds which lack internal deformation or disaggregation, and dip away from the canyon axis (**Figure 8**).

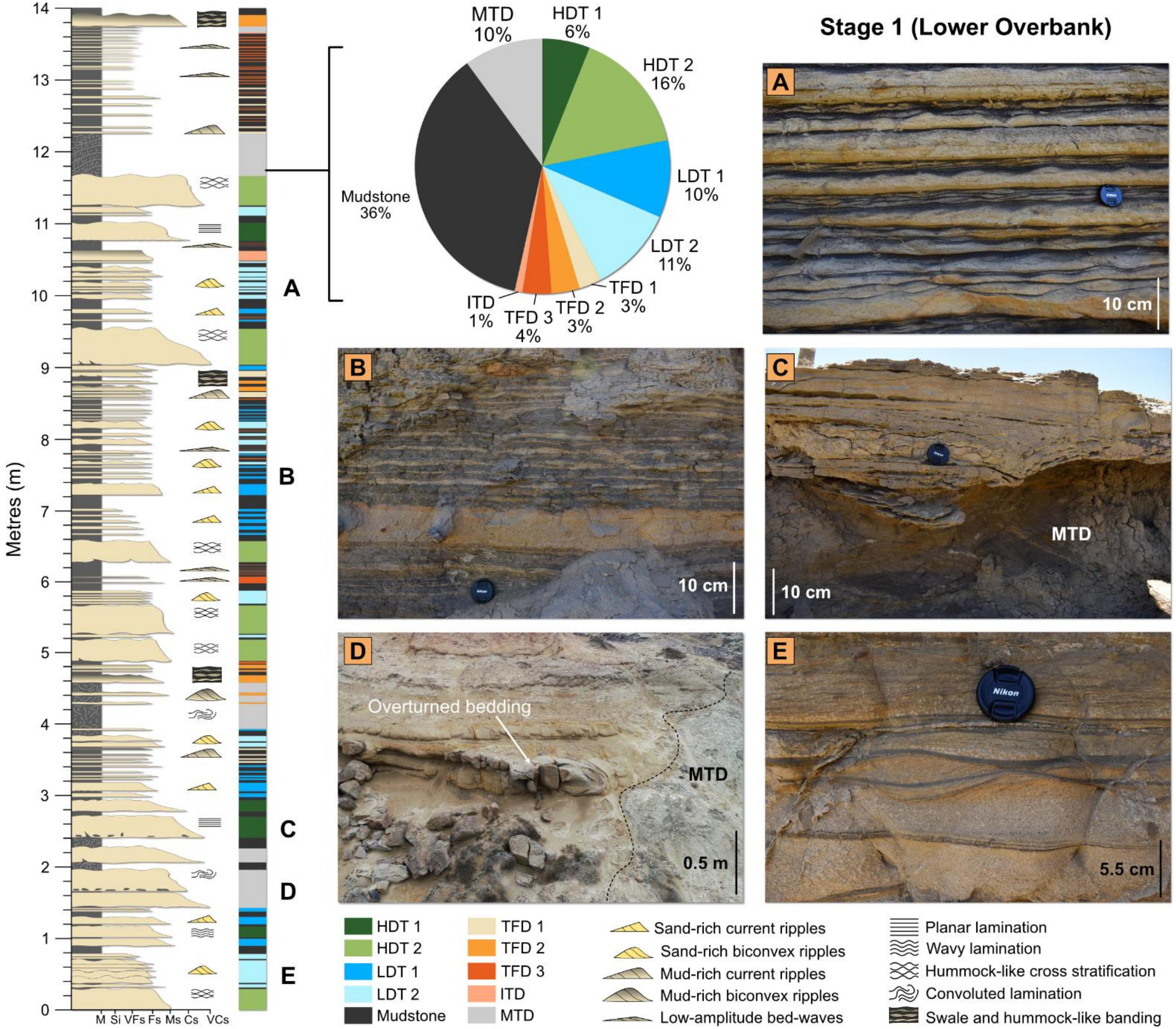

Figure 7. Composite log, bed type proportions and representative photographs through the lower overbank section (Stage 1). (A) LDT 2 beds with structureless and biconvex ripple divisions. (B) Structureless LDT 1 bed which passes into sandy starved ripples. (C) HDT 1 bed thickening into an MTD. (D) Overturned bedding against an MTD at the canyon margin. (E) LDT 2 beds containing sand-rich biconvex ripples. HDT, high-density turbidite; LDT, low-density turbidite; TFD, transitional flow deposit; ITD, internal tide deposit; MTD, mass-transport deposit.

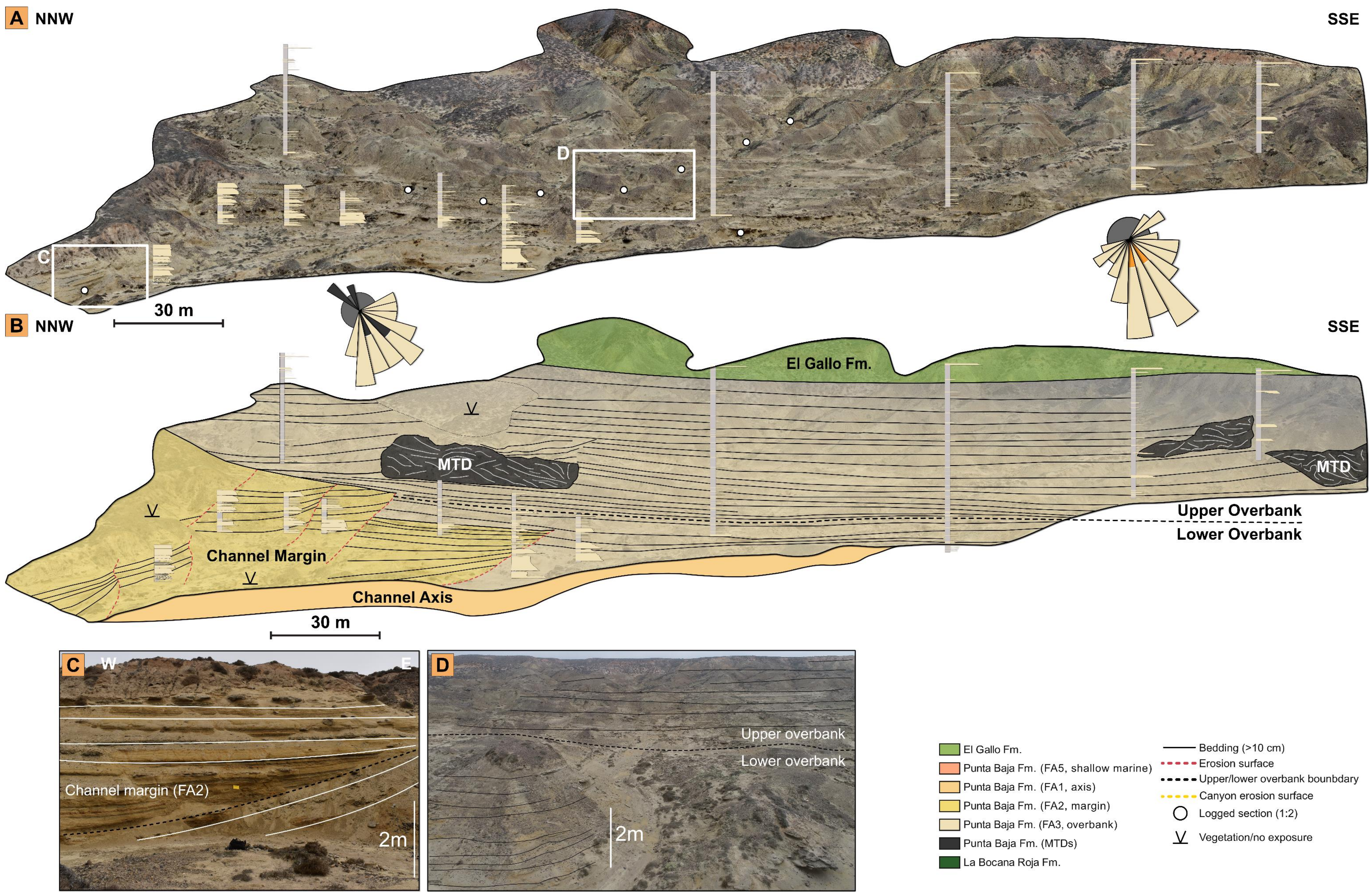

480 **Figure 8**. (A) UAV-captured photogrammetric model of channel margin, lower and upper overbank packages of the Punta Baja canyon-fill, with sedimentary logs projected onto the model. (B) Correlation panel of the margin and overbank packages, with drawn interpretations of the constituent beds, highlighting their lateral and stratigraphic variability. (C) Photograph of medium- to thick-bedded sandstone packages interpreted as a channel margin deposit. (D) Photograph of the confined overbank showing the differences in bed thickness and grain-size between the lower and upper overbank stages. Panel location is shown in Figure 2B. Rose diagrams are oriented with respect to the panel.

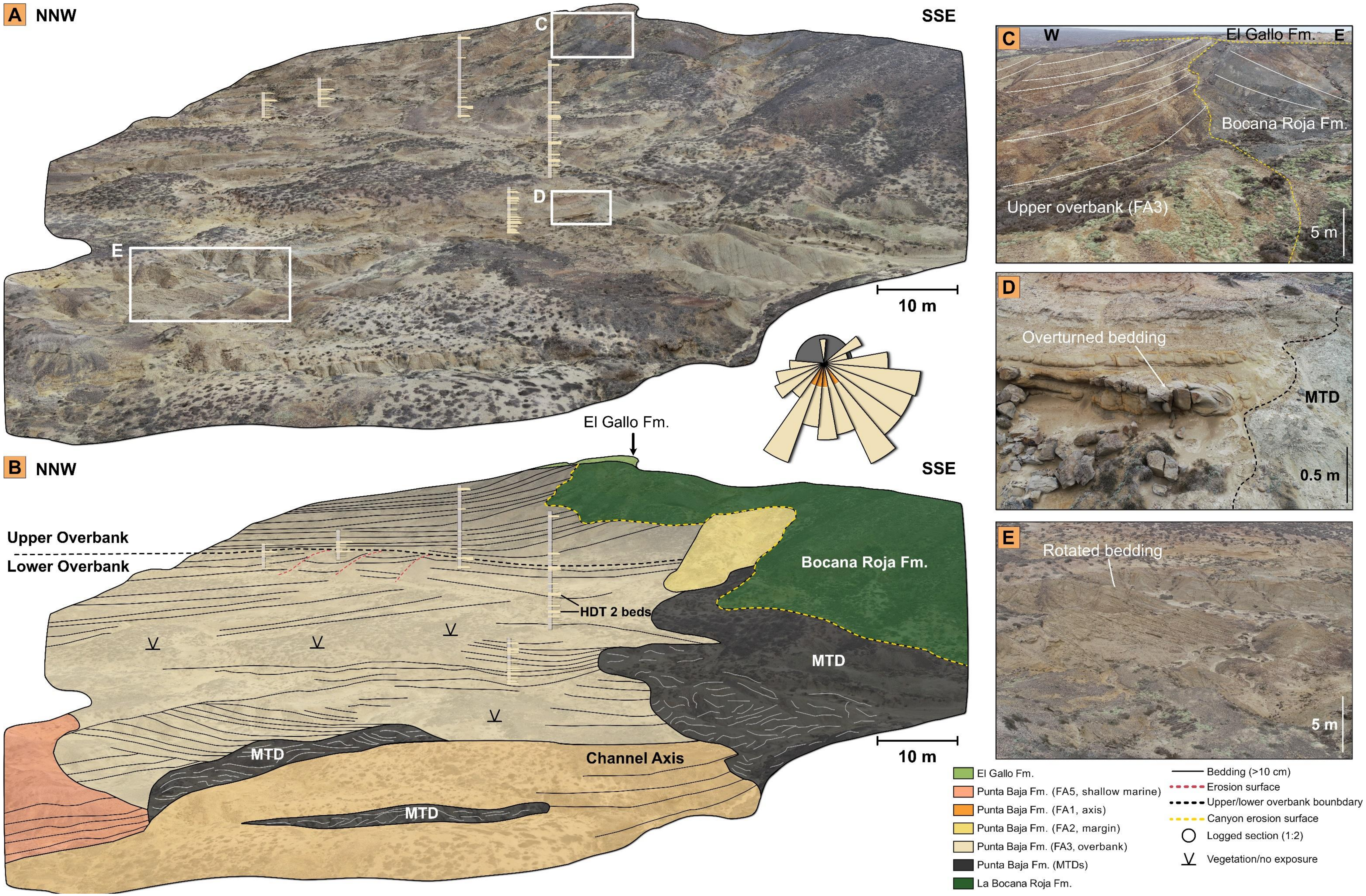

481 **Figure 9**. (A) UAV-captured photogrammetric model of the lower and upper overbank packages of the Punta Baja Formation near the canyon margin, with sedimentary logs projected onto the model. (B) Correlation panel of the overbank section, with drawn interpretations of the main package types, highlighting the lateral and stratigraphic variability of their constituent beds and their interactions with the canyon wall. (C) Photograph of upper overbank packages onlapping onto the canyon wall (Bocana Roja Fm.) and planed off by the overlying El Gallo Fm. (D) Photograph of beds within the lower overbank packages. Beds have been overturned with proximity to MTDs, which were caused by canyon margin failure. (E) Photograph of lower overbank thin-bedded packages which have been rotated due to lateral migration of the channel axis. Location of the panel is shown in Figure 2B. Rose diagrams are orientated with respect to the panel.

Stage 2 (Upper overbank)

Stage 2 (12-28 m thick) represents the upper overbank (**Figure 3**) and sees a marked change in the proportion of observed bed types when compared to Stage 1; TFDs are more common, with fewer HDTs and LDTs (**Figure 10**). Thin-bedded packages of LDTs and TFDs in-between HDT beds have distinct fining- and thinning-upwards trends (**Figure 10**) and decay in thickness and grain-size away from the canyon axis to onlap onto the canyon margin towards the east (**Figure 9**). Stage 2 is more mud-prone than Stage 1 (**Table 2**; sand-to-mud ratio of 41:59). Sandstone beds are thinner (average = 2.6 cm), less variable in thickness (0.1-30 cm), and finer grained (**Table 2**). Overall, palaeocurrent directions from ripples and grooves are towards the south, with a narrower range of directions and fewer examples of palaeocurrent reversals than observed in the lower overbank (**Figure 2A**).

TFDs comprise ~27% of the total measured thickness of Stage 2, while turbulent flow beds (LDTs and HDTs) comprise ~10% (**Figure 6C**). TFD 1 beds are most common with an even stratigraphic distribution throughout Stage 2, with some clustering of thicker beds near aggradationally stacked channel-fills to the west of the upper overbank (**Figure 11**). With lateral distance away from channel-fills, the proportion of TFD 1 beds decreases, and beds gradually become thinner and muddier, before they transition into TFD 2 and 3 beds over a distance of ~ 100 m (**Figure 11**). TFD 2 beds form discrete clusters across the upper overbank and become more widely dispersed in areas away from channel-fills (**Figures 10 & 11**). TFD 3 beds occur in thinner bedded mud-rich packages, either interspersed between other TFD beds, or isolated within thicker (1 – 2 m) mudstone packages (**Figure 11**). The number and thickness of TFD 3 beds increase upwards so that they are the most common bed type in the most distal areas of Stage 2 at locations near the canyon margin, towards the top of the upper overbank (**Figure 10**).

LDT beds comprise ~7% of the total measured thickness of Stage 2 (**Figure 6C**). LDT 1 beds are clustered near the base of the upper overbank stage, near sand-rich channel margin deposits, while LDT

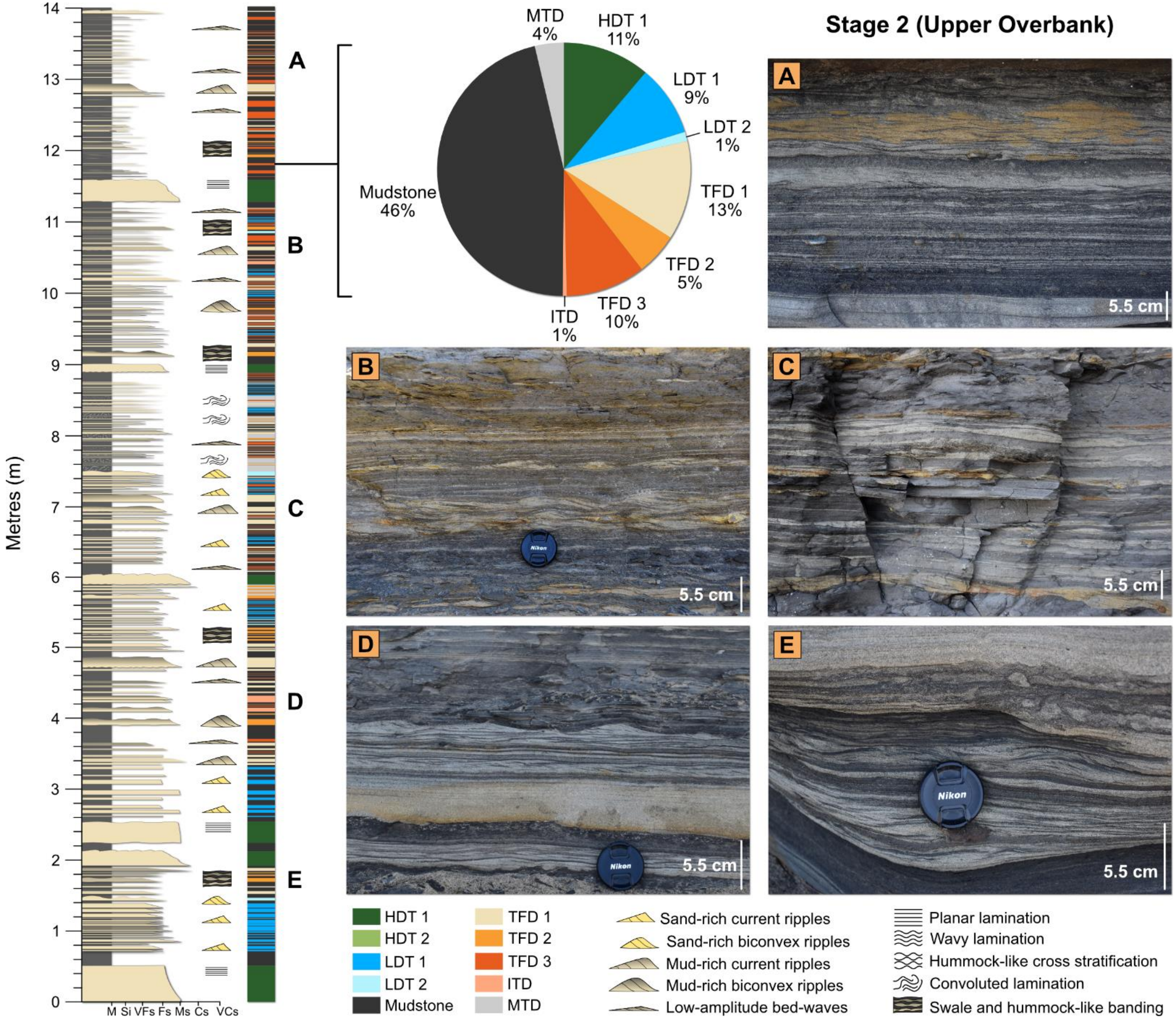

Figure 10. Composite log, bed type proportions and representative photographs through the upper overbank section (Stage 2). (A) TFD 3 bed containing LABWs overlain by a TFD 1 bed containing mud-rich current ripples. (B) TFD 1 beds comprising a basal division of mud-rich current ripples before passing into a division of longer, thinner low-amplitude bed-waves and starved ripples. (C) TFD 1 beds with large mud-rich ripples. (D) ITD bed showing reworking of a (sand-rich) sediment gravity flow deposit by internal tides, characterised by 'rhythmic' thin-thick lamination and starved ripples. (E) TFD 2 beds, demonstrating sandstone-mudstone banded sets and mud-rich ripples. HDT, high-density turbidite; LDT, low-density turbidite; TFD, transitional flow deposit; ITD, internal tide deposit; MTD, mass-transport deposit; LABW, low-amplitude bed-wave.

2 beds are infrequently observed near sandier packages (**Figure 11**). LDT beds appear to transition laterally and vertically into TFD 1 beds with distance from the canyon axis (**Figure 11**).

HDTs comprise ~8% of the total measured thickness of Stage 2 (**Figure 6C**). HDT 1 beds still occur as outsized, laterally continuous marker beds that truncate thin-bedded packages but are typically thinner and less erosive than Stage 1 HDTs (**Figure 8**). They are evenly distributed throughout the upper overbank but become thinner and finer towards distal areas and the top of the overbank (**Figure 10**). HDT 2 beds are rare and are clustered at the base of the upper overbank. MTDs are rare (~3%), and commonly occur as slides, where thin-bedded TFD packages are rotated towards the canyon axis, or as debrites, which occur as thin, laterally discontinuous intervals that extend across the upper overbank. ITDs (~7%) were observed on the western side of the canyon-fill, interspersed between channel margin deposits and mud-rich, thin-bedded packages of the upper overbank (**Figure 10E**).

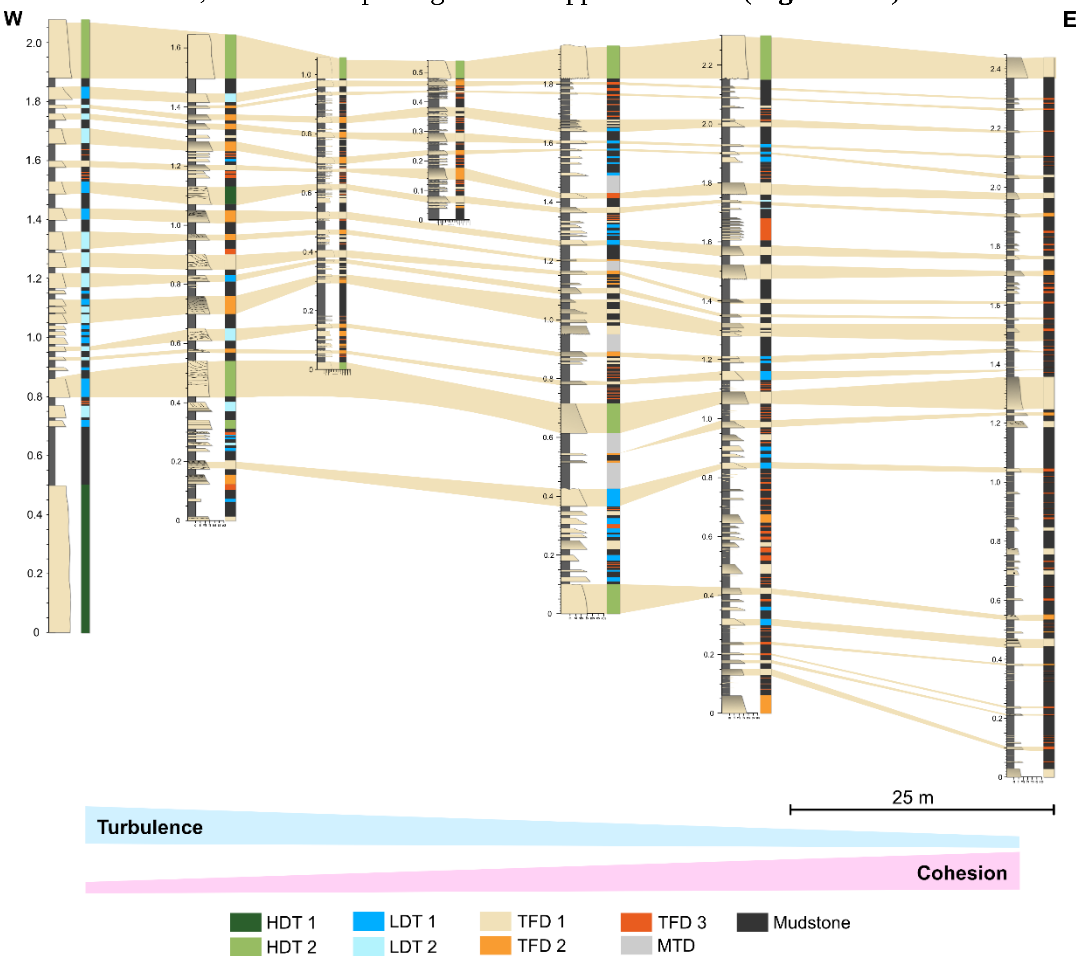

Figure 11. Bed-scale correlation panel of a representative 2-metre section from the upper overbank highlighting the across-strike distribution and lateral transitions of the different bed types over a distance of 100-200 metres. HDT, high-density turbidite; LDT, low-density turbidite; TFD, transitional flow deposit; ITD, internal tide deposit; MTD, mass-transport deposit.

CANYON EVOLUTION AND CONFINED OVERBANK DEVELOPMENT

Channelisation and subsequent backfilling were dominant processes during the evolution of the Punta Baja canyon-fill. The observation of abrupt and frequent vertical and lateral facies changes is characteristic of the fill as a whole (**Figure 3**) and define a system where the active conduit periodically migrated laterally and obliquely. Conglomerates and sandstones of the channel axis (FA1) represent channelised deposition, where flows were confined to channels and the axial gradient was sufficient to transport gravel-sized sediment downslope (Boehlke and Abbott, 1986). The preservation of the overbank on the eastern margin of the canyon-fill records the aggradational stage of the canyon's evolution, following an earlier phase of incision and almost complete sediment bypass (Stevenson et al., 2015), represented by the observation of coarse-grained lag deposits in the channel axis (Figure 3; Bouwmeester et al., 2024). Westward lateral migration of channels and gradual widening of the canyon, coupled with a decrease in the slope gradient from mass-transport deposition promoted the local onset of canyon floor aggradation and the development of overbank accommodation (Bouwmeester et al., 2024). As the canyon aggraded, flows that were transporting sediment through channels (FA1) were stripped and overspilled into the overbank. Further erosion and entrenchment of the axis likely resulted in flow partitioning due to the elevation different between the lower high-density and upper low-density parts of stratified flows (e.g. Piper and Normark, 1983; Peakall et al., 2000; Keevil et al., 2006). Axial channel migration is evident based on observations of westward-cutting and oblique aggradation of sand-rich channel margin deposits (**FA2, Figure 3**). In addition, the asymmetry of the canyon-fill suggests that the axis, on the whole, migrated obliquely westward which would contribute to the upward thinning and fining trends observed in the upper overbank (Stage 2).

The net-aggradation of the canyon demonstrates a highly efficient conduit that eroded and bypassed sediment in an entrenched axis while an overbank was constructed. The conglomeratic channel axis-fill with sandstone-filled scours suggests that flows bypassed grainsizes up to pebble/cobbles through the axis, with the higher sand- and mud-bearing parts of flows partially stripping and overspilled onto the overbank (Bouwmeester et al., 2024). The abundant erosional structures, sharp-topped HDTs and downslope palaeocurrent directions in some of the overbank deposits also suggest that at least some of the overbanking flows bypassed sediment downslope.

DISCUSSION

A new model for the evolution of canyon-confined overbanks

Lower overbank stage

The lower overbank stage records the early stages of canyon aggradation. The high sand-to-mud ratio, variable bed thicknesses and wide grain-size distribution (**Figure 6**) suggests that the lower overbank received flows of varying magnitudes that were fully confined within the canyon. The lower overbank is therefore interpreted as a high energy environment where the dominant flow processes are fully turbulent sediment gravity flows (**Figure 12**). HDTs represent infrequent, higher magnitude flows that overspilled adjacent channels to deposit medium-bedded turbidites, and LDTs represent lower magnitude flows which deposited thin-bedded turbidites, where the dilute upper parts of flows were either stripped or overspilled from channels into restricted overbank accommodation. (Piper and Normark, 1983; Hiscott et al., 1997; Peakall et al., 2000; Hansen et al., 2015).

The consistent thickness and lateral continuity of most HDT beds suggest that higher magnitude, fully turbulent flows were able to extend completely across the lower overbank to reflect and deflect against the canyon margin topography (**Figure 12**). The lateral transition from HDT 1 beds into HDT 2 beds within 10-20 metres of the canyon margin support an interpretation of flow transformation from an initially unidirectional flow to a combined flow, where upon incidence with the base of the canyon wall, an incoming parental flow becomes stripped, generating thin, dilute multidirectional flows which propagate onto the canyon wall surface and collapse downward (Keavney et al., 2024). These flows are then superimposed onto the initial parental flow which generates a combined flow in the absence of an oscillatory component (Keavney et al., 2024), and reworks beds into the dune-scale hummock-like bedforms, as observed at the tops of HDT 2 beds. The abrupt pinch out of HDT 2 beds (**Figure 9**) suggest that the lower parts of higher magnitude flows were not able to run up the canyon wall surface, while clustering of thinner LDT 2 beds above HDT 2 beds are possible records of the collapsing, multidirectional flows that propagated onto the canyon wall, and formed their own deposits (**Figure 7**). The even stratigraphic distribution of HDT 2 and LDT 2 beds near the canyon margin (**Figure 7**) suggest that combined flows were repeatedly generated from reflection and deflection against the canyon wall, suggesting that the lower overbank was highly confined by steep canyon walls. The variable palaeocurrent directions and flow reversals in near the canyon margin (**Figure 2A**) demonstrate flow complexity on incidence with the canyon wall, suggesting a particularly rugose surface, or that flows were possibly stripped from different parts of evolving channel bend resulting in different incidence angles of flows with the canyon wall.

The observations of LDT 2 beds away from the canyon margin (**Figure 6C**) support interpretations of seabed topography. Here, lower magnitude flows were likely reflected, deflected and ponded against evolving erosional and depositional relief, such as scour surfaces and MTD topography to set up combined-oscillatory flows (**Figure 12**). Scour surfaces were likely formed by erosive, higher magnitude flows that reworked the overbank, while MTDs were sourced from repeated deflection of flows against canyon walls, causing erosion, oversteepening and flank collapse (**Figure 9**). This resulted in mud-rich debris flows that extended across the canyon floor, forming complex relief that resulting in deflection and ponding of subsequent flows. The discontinuous wedge-shaped HDT beds above MTDs are interpreted as confined deposition from high magnitude flows. Clusters of TFD 2 beds above MTDs are records of combined transitional flow transformation from turbulent to laminar as low magnitude flows passed over the mud-rich substrate, entrained cohesive mud and deflected against MTD relief. Slumps and slides near channel-fills likely represent collapse of thin-bedded packages from undercutting of the overbank from oblique migration of channels (Boehlke and Abbott, 1986).

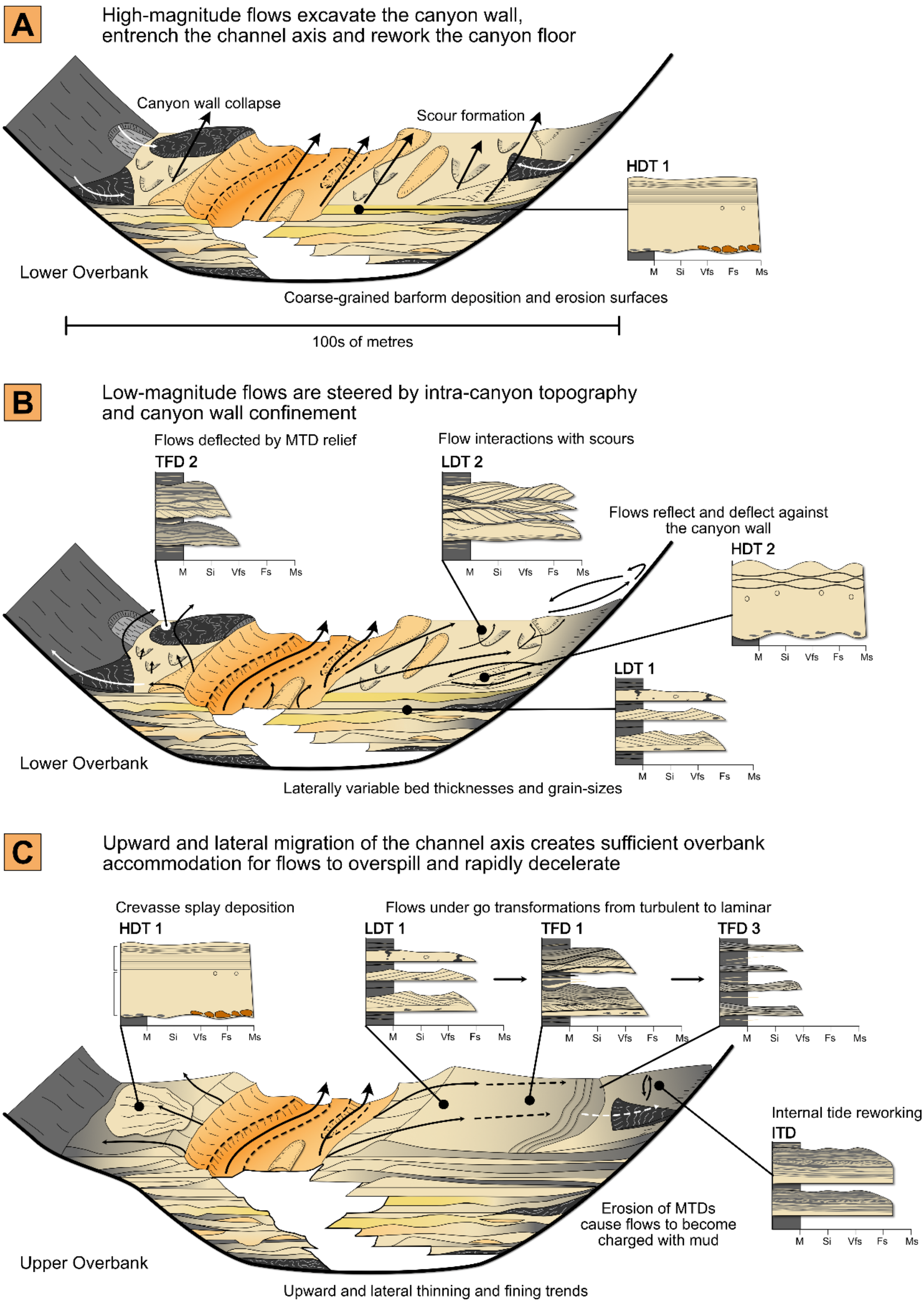

Figure 12. Conceptual diagram of a canyon setting, showing the locations where different flow transformations and bed types are expected to form. (A) Lower overbank stage where high-magnitude, erosional flows are the dominant process. (B) Lower overbank stage where lower magnitude flows are affected by complex canyon topography. (C) Upper overbank stage, where canyon widening creates sufficient accommodation for flow to overspill and transform between turbulent and laminar states. HDT, high-density turbidite; LDT, low-density turbidite; TFD, transitional flow deposit; ITD, internal tide deposit.

599

Furthermore, the observation of LDT 2 beds at the base of the lower overbank point to flow interactions with remnant topography resulting from the westward lateral-oblique migration of the channel axis during the initial stages of overbank aggradation. Gradual upward transitions from combined flow beds (LDT 2 & HDT 2) to LDT 1 beds (**Figure 7**) possibly support healing of topography such that successive flows were less affected by increasingly subtle seabed topography. LDT 1 beds, therefore, represent lower magnitude turbulent flows that were able to run out across the overbank with little topographical interference.

The general paucity of TFDs across Stage 1, apart from some above mud-rich MTDs, is likely due to a lack of mud-rich substrate available for flows to entrain cohesive mud. The initial substrate would have comprised conglomeratic and sand-rich channel-fills, and later sand-rich HDT beds (Boehlke and Abbott, 1986; Kane et al., 2022). Furthermore, the larger scale confinement of the lower overbank also likely prevented flows from running out and decelerating fully before interaction with the canyon wall, thereby inhibiting transformations from turbulent to laminar flows. The transition to the upper overbank is marked by an increasing proportion of TFDs towards the top of the lower overbank, and a notable decrease in the thickness, and number of HDTs.

Upper overbank stage

The upper overbank stage represents later stages of canyon aggradation (**Figure 12**). Further oblique migration of the channel axis widened the canyon thereby increasing the accommodation available for flows to overspill into the overbank (Bouwmeester et al., 2024). The lower sand-to-mud ratio, thinner and less variable bed thicknesses, and a narrower grain-size distribution (**Figure 6**) suggests that the upper overbank received smaller but more regular flow magnitudes than the lower overbank, supporting an interpretation of an overall lower energy and more stable environment of deposition (**Figure 12**). Transitional flows are more common than cohesionless, turbulent flows (**Figure 10**), demonstrating that the upper overbank was conducive to flow transformations through the balance of cohesive and turbulent forces.

TFD 1 beds represent unidirectional flow transformation from an initially turbulent flow to a turbulence-modulated transitional flow. Their even distribution near channel-fills demonstrate that flows experienced abrupt decreases in confinement as (parts of) flows were stripped or overspilled channels (Peakall et al., 2000; Hansen et al., 2015), and decelerated rapidly. The higher preservation of channel margin deposits in the upper stage (**Figure 8**), suggests a higher channel sinuosity and therefore more abrupt losses in confinement from overspill. Deeper entrenchment of the channel axis and higher relief (Bouwmeester et al., 2024) may further promote abrupt losses in confinement, thereby driving flow transformations. Given this, transitions from turbulent flows to transitional flows were possibly enhanced by stronger flow partitioning, where dilute upper parts of overspilling flows became relatively more enriched in mud, as the denser sand-rich fraction of flows remained confined to channels. This ultimately resulted in increased cohesion in decelerating flows, promoting turbulence modulation and the generation of mixed grain-size bedforms. Flows would have become more cohesive from entrainment of mud-prone substrate in the upper overbank. Due to the higher aspect ratio of the canyon, it is possible that more mud was deposited and preserved in the upper overbank compared to the lower overbank stage when it was more likely bypassed or resuspended by high magnitude flows. Additional mud-rich substrate was likely derived from debris flows from erosion and collapse of unstable canyon walls. The upward and lateral transitions from sand-rich turbidites (LDT 1 beds) near channel-fills indicate the initial phase of transformation from fully turbulent, non-cohesive flows to transitional flow conditions.

The gradual thinning and lateral transition from TFD 1 beds through TFD 2 to TFD 3 beds with lateral distance from channel-fills (**Figure 11**), point to lateral flow transformations from LTPF to UTPF conditions across the upper overbank as flows escaped channel confinement and decelerated but remained within the confines of the canyon. TFD 1 beds transition to TFD 3 beds over a distance of 100 to 200 m, demonstrating particularly rapid flow transformations. The rate of flow transformation is more rapid than other depositional environments in previous studies, such as internal levées in a mid-slope settings, where flows transform over 1 to 2 km (Taylor et al., 2024), and distal fan fringe environments, where flows are shown to transform over 2 to 3 km (Baker and Baas, 2020).

The distinct clusters of TFD 2 beds (**Figure 11**) indicate where flows transition as they pass over mud-prone substrate and interact with subtle seabed topography, such as scour surfaces or relief generated by mud-rich debris flows. Their mudstone caps may suggest ponded deposition in topographic lows (Pickering and Hiscott, 1985; Haughton, 1994), which further suggests the presence of MTD relief and scour surfaces. The observation of thick TFD 2 beds in areas close to the canyon margin implies that decelerated flows were just about able to reflect and deflect off the canyon walls, while thinner TFD 2 beds in these areas suggest that flows became increasingly susceptible to topographic influence as they decelerated and thinned (Kneller and Buckee, 2000).

The high proportions of TFD 3 beds in the most distal parts of the upper overbank represent the lateral extent of overspilling unidirectional transitional flows (**Figure 11**), which suggests that the majority of flows did not interact with the canyon margin. The upward increase in the proportion of TFD 3 beds with respect to TFD 1 and 2 beds (**Figure 10**), could represent increased channel relief with time (Hiscott et al., 1997; Pirmez and Imran, 2003), wider overbank accommodation from channel migration (Maier et al., 2012; Hansen et al., 2015) or decreases in the magnitude of SGFs as the system aggraded (Kneller, 2003). ITDs were almost exclusively observed in the upper overbank (**Figures 10D & E**). This is likely because it is a lower energy environment with an availability of sand from overspilling low magnitude flows to rework into internal tide deposits. The removal of deposits by erosive, higher magnitude flows is less likely given their scarcity in the upper overbank section.

HDTs are fewer and more widely interspersed throughout the upper overbank which implies that higher magnitude flows were infrequent, or that flows were increasingly confined to channels due to higher channel relief as the system aggraded. Tabular-shaped HDT 1 beds thin with lateral distance from channel-fill and pinch out abruptly, suggesting that higher magnitude flows formed crevasse splays from breaching channel confinement, most likely at the outer bend of the channel (Lowe et al., 2019). The few instances of HDT 2 beds at the base of the upper overbank record higher magnitude flows that were able to interact with the canyon margin at the transition between the depositional stages.

The dynamic nature of confined overbank successions

The bed types and their distributions described here show that the Punta Baja canyon overbank was a highly dynamic environment with a range of flow types, transformations and complex interactions with topography that evolved through time. This resulted in a heterogenous fill which demonstrates that interpretations of canyon-confined overbanks require consideration of individual flows and their three-dimensional interactions with topography, rather than a sole assessment of depositional environment.

Currently, models that describe confined overbank successions are derived from channel-levée systems from mid- to lower slope settings and do not fully consider canyon settings. They describe depositional terrace deposits (Hansen et al., 2015; Hansen et al., 2017), and internal levées (Babonneau et al., 2004; Dykstra and Kneller, 2009; Kane et al., 2009; Kane and Hodgson, 2011; Morris, 2014), which are distinguished on the basis of their external morphology and internal sedimentological characteristics (Hansen et al., 2015). Depositional terrace deposits are flat-lying, sheet-like deposits formed by turbulent flows that overspill channels, extend across the entire conduit, and reflect and deflect against confining surfaces (Hansen et al., 2015). Internally, they comprise packages of thin-bedded turbidites with variable bed thicknesses that show minimal lateral variation in sandstone proportion with distance away from channel-fills (Hein and Walker, 1982; Schwarz and Arnott, 2007; Hansen et al., 2017). Conversely, internal levées are wedge-shaped features that, unlike terrace deposits, form when there is sufficient space within the conduit for flows to overspill, decelerate and deposit the majority of the suspended sediment before reaching the confining surface (Hansen et al., 2015; Hansen et al., 2017). When compared to depositional terrace deposits, internal levées have less variable bed thicknesses within thin-bedded packages and exhibit upward thinning- and fining trends (Beaubouef, 2004; Kane et al., 2009; Kane and Hodgson, 2011).

In some ways, the lower overbank stage documented here acts like a terrace deposit, with the terrace formed by the oblique upward migration of channels. Furthermore, the confined nature of the bounding surface meant that flows were able to reflect and deflect against the canyon wall. Similarly, the upper overbank stage meets some of the criteria for internal levées, with discrete thin-bedded packages that thin- and -fine upwards and laterally towards the canyon margin. However, while the lower and upper overbank stages share some broader characteristics with terrace deposits and internal levée models, associated with more distal channel-levée complexes, they only invoke stable flow conditions, such as waning turbulent flow processes in an otherwise dynamic environment where flow transformations are common (**Figure 12**). Furthermore, they only consider lateral changes from channel to master confining surface and do not fully consider the three-dimensional shape and distribution of beds and packages. Whilst there may be a general trend from more depositional terrace-like stage to more internal levée-like stage as the canyon is filled, this bimodal approach hides a lot of the variability that comes from evolving erosional and depositional topography, especially in three dimensions during evolution of the canyon.

As demonstrated above, canyon-confined overbanks are highly dynamic environments due to a wide range of erosional and depositional bedforms and mass transport deposits which generate complex relief (**Figure 12**). The dynamics of channels within canyons means that the nature of the overbank shifts with respect to the channel axis throughout time. This results in a wide range of flow types and deposits which respond to channel axis movements, therefore limiting the development of discrete architectural

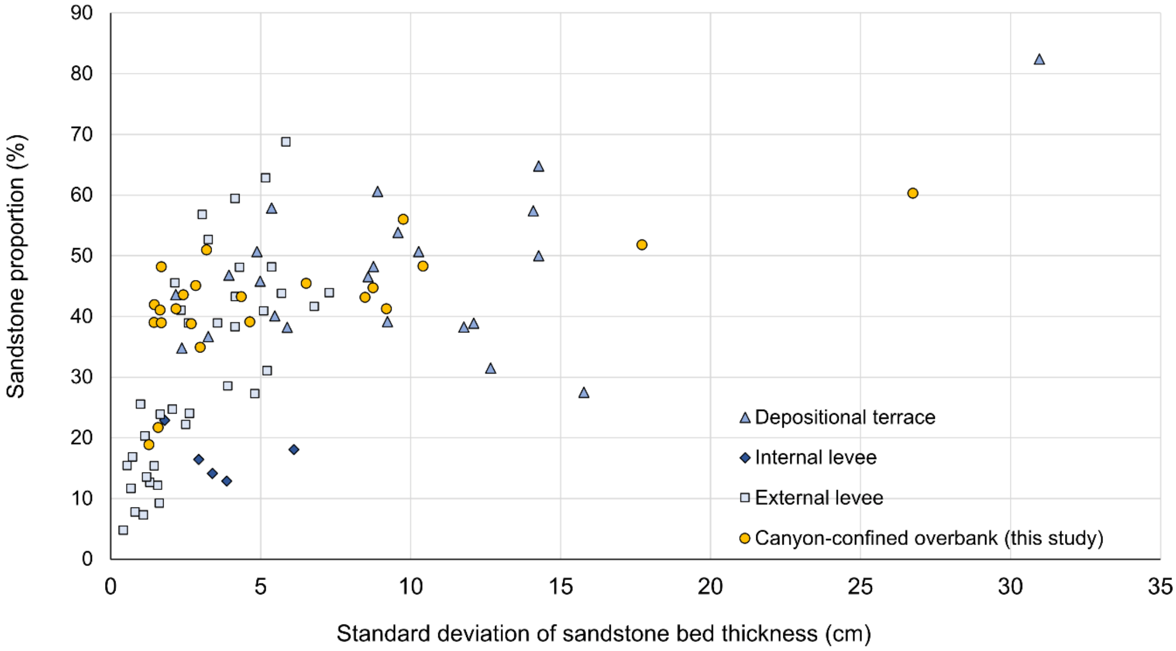

Figure 13. Cross plot of the standard deviation of sandstone bed thickness against sandstone proportion for a canyon-confined overbank (this study), compared with the data from Hansen et al. (2017).

elements. Ultimately, using end-member models to subdivide confined overbanks in submarine canyons is too limiting for palaeoenvironmental reconstructions because there are many architectural connotations within submarine canyons to label discrete thin-bedded depositional environments.

A proposed criterion for differentiating thin-bedded depositional environments has been to use sandstone bed thicknesses. **Figure 13** shows a cross plot of the standard deviation of sandstone bed thickness against sandstone proportion for each log from this study, compared with data from Hansen et al. (2017). However, as shown in **Figure 13**, the data from the Punta Baja overbank plots across all fields of terrace deposits, internal levée and external levée, showing that these environments are simply too dynamic to apply a single depositional environment based on averaged values of bed thickness and sandstone proportion.

Furthermore, existing models of terrace deposits and internal levées are mostly derived from channel-levée complexes from mid- to lower slope settings where channel-belts have some degree of overspill and form thick external levées outside of the conduit. This has the effect of filtering out the upper fine-grained component of flows, thus restricting the range of deposits that form within the conduit. In canyons, flows are fully confined by steep erosion surfaces with little-to-no external levée generation. Therefore, unfiltered flows within canyons are likely to be more variable and dynamic in their sedimentological characteristics than overbanks of more distal channel-levée systems, further complicating potential interpretations of internal levées or terrace deposits.

Therefore, overbank environments, especially those confined within canyons must be interpreted from changes in palaeoenvironment linked to the evolution of the system as a whole. If discrete environments are labelled primarily based on their geometries as in the case of depositional terrace and internal levée models, then their utility as archives of palaeoenvironmental change could be hindered. This study stresses that the overall evolution of the confined overbank must be assessed with relation to channel-fills, their three-dimensional nature and their palaeogeographic context.

Interpretation of internal tide deposits from the ancient rock record

Internal tides have been shown to resuspend and transport sediment in submarine settings worldwide (Shepard and Marshall, 1969; Shepard et al., 1979), but in the absence of recognition criteria, their deposits have not been unequivocally identified in the rock record. In fact, their interpretation has long been contested (e.g., Shanmugam and Wang, 2014), due to a previous lack of studies that link direct flow monitoring of modern internal tides to cored deposits. However, this is no longer the case as recent studies have successfully verified sedimentological observations from sediment traps and cores with direct measurements of internal tides from the Whittard Canyon, NE Atlantic margin (Soutter et al., 2024); Monterrey Canyon, California (Maier et al., 2019); and Logan Canyon, Eastern Canada (Normandeau et al., 2024). Attempts can now be made to interpret internal tide deposits from ancient canyon-fills to support palaeoenvironmental reconstructions.

Linked modern observations of internal tides comprise sharp-topped sandstone beds with abrupt grain-size breaks from sand to mud, planar/wavy silt and fine sand laminasets which form thick-thin sand-mud couplets (rhythmites) with normal and inverse grading, and mud-draped starved ripples (Maier et al., 2019; Normandeau et al., 2024). These studies agree that such sedimentary structures are deposits of internal tides, characterised by waxing and waning tidally-forced flows that resuspend and redistribute sediment on bed tops. Other structures which are linked to internal tides but rarely preserved are bidirectional ripples (May and Warme, 2007), which likely represent flow reversals from tidally-influenced transport up-canyon (flood), although stronger down-canyon transport (ebb) could explain the rarity of preserved bi-directional ripples, because downslope currents would resuspend sediment deposited under weaker up-slope currents and remove up-canyon facing foreset laminae (He et al., 2011; Normandeau et al., 2024).

Differentiating the deposits of internal tides from other processes that generate mixed grain-size bedforms, such as transitional flows is challenging. Similarities between internal tide deposits and transitional flows include alternating sandstone-mudstone laminae and banded sets and discontinuous starved laminae. However, the cyclical nature of laminae and banded couplets and the thick-thin transition between ‘double bands’ bears closer resemblance to documented internal tide deposits (Soutter et al., 2024). Furthermore, the lack of continuous transitions between different bedforms (i.e. mud-rich current ripples to low-amplitude bed waves) in a single deposit (**Figure 10D**) suggest that these deposits did not undergo flow transformations.

Most of the facies reported from modern systems as indicative of internal tide deposits (apart from bidirectional ripples) are observed in the interpreted ITDs from the upper overbank , thereby suggesting that internal tides were present and strong enough to transport sediment in the Punta Baja canyon during the Cretaceous. However, the proportion of these deposits is low (~9% of total measured sections). This is likely due to complete reworking by sediment gravity flows which overspilled into the overbank, or by bioturbation which reworks and destroys laminae and banded sets (Li et al., 2019; Normandeau et al., 2024). In some ITDs observed in the Punta Baja overbank, the presence of thin, discontinuous laminae, coupled with a mottled texture above laminasets might indicate where deposition was interrupted by partial reworking of sediment by organisms. Therefore, the preservation of internal tide deposits requires higher sedimentation rates during laminaset deposition to outpace the rate of bioturbation. Dykstra (2012) suggests that increased sediment availability could lead to higher preservation potential of internal tide deposits. In canyons, storm events have been shown to increase suspended sediment concentrations (Li et al., 2019), which have been linked to increased preservation potential of internal tide deposits (Yang et al., 2020). Another mechanism could be the influence of earthquakes given the forearc basin setting, which would increase suspended sediment concentrations. These events are likely factors for the preservation of ITDs in the Punta Baja canyon.

CONCLUSIONS

This study presents an exceptional example of an exhumed canyon-confined overbank from the Mesozoic Peninsular Ranges Forearc, Mexico. Detailed outcrop logs and photogrammetric models has revealed that the overbank was an especially dynamic environment where a variety of different bed types point to progressive transformations in flow properties that evolved throughout the evolution of the canyon. The overbank can be subdivided into two distinct depositional stages, which constitute the stratigraphically lower and upper overbank successions. These stages are distinguished based on differences in the proportion and distribution of bed types, their sand: mud ratio, variations in bed thicknesses, grain-size, palaeoflow directions and depositional architecture.

The lower overbank contains a significant proportion of sandstone (sand-to-mud ratio of 50:50), with variable bed thicknesses, palaeocurrent directions and a wide grain-size distribution (medium silt to gravel), with a tendency toward coarser grain-sizes when compared to the upper overbank. These observations point to a wide range of unfiltered flows that overspilled from channels. Thick sandstone beds contain distinct hummock-like bedforms, representing high magnitude combined flows that repeatedly deflected and reflected against the high relief canyon margin, suggesting complete confinement within the conduit. Locally, thinner beds are disrupted by slides, debrites and scour surfaces on the canyon floor.

As the canyon system matured, constituent channels migrated obliquely to the west. Here, the character of the overbank changes, developing distinct fining- and thinning-upward packages that decay in thickness and grain-size away from the channel axis. Packages are more mud-rich and beds contain distinct mixed grain-size bedforms that demonstrate smaller magnitude, rapidly decelerated transitional flows that entrained mud-rich substrate and mostly failed to interact with the canyon margin. In more quiescent parts of the upper overbank, beds contain rhythmic bundles of silt-rich, mud-draped bedforms, which are interpreted to be the product of sediments reworked by internal tides. This is the first detailed study of a fine-grained fill in an ancient ocean-facing submarine canyon. Canyon-confined overbanks offer a diverse fill, with flow transformations that demonstrate a complex balance between erosion and deposition, and an absence of discrete internal levée or depositional terrace elements that have been identified in more distal confined overbank settings.

AKNOWLEDGEMENTS

The SLOPE 5 consortium (BP, Aker BP, CNOOC International, Hess, Murphy, Neptune Energy, Petrobras, Vår Energi, Wintershall DEA, Woodside) are thanked for their financial support.

DATA AVAILABILITY STATEMENT

REFERENCES CITED

Allen, J. R. L., 1971, Instantaneous sediment deposition rates deduced from climbing-ripple cross-lamination: J. Geol. Soc., v. 127, no. 6, p. 553-561.

Allen, J. R. L., 1973, A classification of climbing-ripple cross-lamination: J. Geol. Soc., v. 129, no. 5, p. 537-541.

Allen, J. R. L., 1982, Sedimentary structures, their character and physical basis, Developments in Sedimentology, 1, 2: Amsterdam, Elsevier, p. 593, 663.

Allen, S. E., and Durrieu de Madron, X., 2009, A review of the role of submarine canyons in deep-ocean exchange with the shelf: Ocean Sci., v. 5, no. 4, p. 607-620.

Amaro, T., Huvenne, V. A. I., Allcock, A. L., Aslam, T., Davies, J. S., Danovaro, R., De Stigter, H. C., Duineveld, G. C. A., Gambi, C., Gooday, A. J., Gunton, L. M., Hall, R., Howell, K. L., Ingels, J., Kiriakoulakis, K., Kershaw, C. E., Lavaleye, M. S. S., Robert, K., Stewart, H., Van Rooij, D., White, M., and Wilson, A. M., 2016, The Whittard Canyon – A case study of submarine canyon processes: Prog. Oceanogr., v. 146, no. C, p. 38-57.

Anderson, K. S., Graham, S. A., and Hubbard, S. M., 2006, Facies, Architecture, and Origin of a Reservoir-Scale Sand-Rich Succession Within Submarine Canyon Fill: Insights from Wagon Caves Rock (Paleocene), Santa Lucia Range, California, U.S.A: J. Sed. Res., v. 76, no. 5, p. 819-838.

Archer, A. W., 1996, Reliability of lunar orbital periods extracted from ancient cyclic tidal rhythmites: Earth Planet. Sci. Lett., v. 141, no. 1, p. 1-10.

Ashley, G. M., Southard, J. B., and Boothroyd, J. C., 1982, Deposition of climbing-ripple beds: a flume simulation: Sedimentology, v. 29, no. 1, p. 67-79.

Baas, J. H., and Best, J. L., 2002, Turbulence modulation in clay-rich sediment-laden flows and some implications for sediment deposition: J. Sed. Res., v. 72, no. 3, p. 336-340.

Baas, J. H., Best, J. L., and Peakall, J., 2011, Depositional processes, bedform development and hybrid bed formation in rapidly decelerated cohesive (mud-sand) sediment flows: Sedimentology, v. 58, no. 7, p. 1953-1987.

Baas, J. H., Best, J. L., and Peakall, J., 2016, Predicting bedforms and primary current stratification in cohesive mixtures of mud and sand: J. Geol. Soc., v. 173, no. 1, p. 12-45.

Baas, J. H., Best, J. L., and Peakall, J., 2021a, Rapid gravity flow transformation revealed in a single climbing ripple: Geology, v. 49, p. 493-497.

Baas, J. H., Best, J. L., Peakall, J., and Wang, M., 2009, A phase diagram for turbulent, transitional, and laminar clay suspension flows: J. Sed. Res., v. 79, no. 4, p. 162-183.

Baas, J. H., Tracey, N. D., and Peakall, J., 2021b, Sole marks reveal deep-marine depositional process and environment: Implications for flow transformation and hybrid-event-bed models: J. Sed. Res., v. 91, no. 9, p. 986-1009.

Babonneau, N., Savoye, B., Cremer, M., and Bez, M., 2010, Sedimentary Architecture in Meanders of a Submarine Channel: Detailed Study of the Present Congo Turbidite Channel (Zaiango Project): J. Sed. Res., v. 80, no. 10, p. 852-866.

Babonneau, N., Savoye, B., Cremer, M., Bez, M., Lomas, S. A., and Joseph, P., 2004, Multiple terraces within the deep incised Zaire Valley (ZaïAngo Project): are they confined levees?, Confined Turbidite Systems, 222, Geological Society of London, p. 0.

Baker, M. L., and Baas, J. H., 2020, Mixed sand–mud bedforms produced by transient turbulent flows in the fringe of submarine fans: Indicators of flow transformation: Sedimentology, v. 67, no. 5, p. 2645-2671.

Beaubouef, R. T., 2004, Deep-water leveed-channel complexes of the Cerro Toro Formation, Upper Cretaceous, southern Chile: AAPG Bulletin, v. 88, no. 11, p. 1471-1500.

Bell, D., Stevenson, C. J., Kane, I. A., Hodgson, D. M., and Poyatos-Moré, M., 2018, Topographic controls on the development of contemporaneous but contrasting basin-floor depositional architectures: J. Sed. Res., v. 88, no. 10, p. 1166-1189.

Best, J. L., and Bridge, J. S., 1992, The morphology and dynamics of low amplitude bedwaves upon upper stage plane beds and the preservation of planar laminae: Sedimentology, v. 39, no. 5, p. 737-752.

Bianchelli, S., and Danovaro, R., 2019, Meiofaunal biodiversity in submarine canyons of the Mediterranean Sea: A meta-analysis: Prog. Oceanogr., v. 170, p. 69-80.

Boehlke, J. E., and Abbott, P. L., 1986, Punta Baja formation, a campanian submarine canyon fill, Baja California, Mexico, *in* Abbott, P. L., ed., Cretaceous stratigraphy of western North America, Special Publication 46, SEPM, p. 91-101.

Boulesteix, K., Poyatos-Moré, M., Flint, S. S., Hodgson, D. M., Taylor, K. G., and Brunt, R. L., 2022, Sedimentologic and stratigraphic criteria to distinguish between basin-floor and slope mudstones: Implications for the delivery of mud to deep-water environments: The Depositional Record, v. 8, no. 2, p. 958-988.

Boulesteix, K., Poyatos-Moré, M., Flint, S. S., Taylor, K. G., Hodgson, D. M., and Hasiotis, S. T., 2019, Transport and deposition of mud in deep-water environments: Processes and stratigraphic implications: Sedimentology, v. 66, no. 7, p. 2894-2925.

Bouma, A. H., 1962, Sedimentology of some flysch deposits : a graphic approach to facies interpretation, Amsterdam, Elsevier Pub. Co., 168 p.:

Bouwmeester, M. J., Kane, I., Hodgson, D., Flint, S., Taylor, W., Soutter, E., McArthur, A., Poyatos-Moré, M., Marsh, J., Keavney, E., Brunt, R. L., and Valdez, V., 2024, Evolution and architecture of an exhumed ocean-facing coarse-grained submarine canyon fill, Baja California, Mexico: EarthArXiv.

Brooks, H. L., Ito, M., Zuchuat, V., Peakall, J., and Hodgson, D. M., 2022, Channel-lobe transition zone development in tectonically active settings: Implications for hybrid bed development: The Depositional Record, v. 8, p. 829-868.

Bruhn, C. H. L., and Walker, R. G., 1995, High-resolution stratigraphy and sedimentary evolution of coarse-grained canyon-filling turbidites from the Upper Cretaceous transgressive megasequence, Campos Basin, offshore Brazil: J. Sed. Res., v. 65, no. 4b, p. 426-442.

Busby, C., 2004, Continental growth at convergent margins facing large ocean basins: a case study from Mesozoic convergent-margin basins of Baja California, Mexico: Tectonophysics, v. 392, no. 1-4, p. 241-277.

Busby, C., Smith, D., Morris, W., and Fackler-Adams, B., 1998, Evolutionary model for convergent margins facing large ocean basins: Mesozoic Baja California, Mexico: Geology, v. 26, no. 3, p. 227-230.

Cartigny, M. J. B., Eggenhuisen, J. T., Hansen, E. W. M., and Postma, G., 2013, Concentration-Dependent Flow Stratification In Experimental High-Density Turbidity Currents and Their Relevance To Turbidite Facies Models: J. Sed. Res., v. 83, no. 12, p. 1047-1065.

Clift, P. D., Giosan, L., Henstock, T. J., and Tabrez, A. R., 2014, Sediment storage and reworking on the shelf and in the Canyon of the Indus River-Fan System since the last glacial maximum: Basin Res., v. 26, no. 1, p. 183-202.

Clifton, H. E., 1984, Sedimentation units in stratified resedimented conglomerate, Paleocene submarine canyon fill, Point Lobos, California, Sedimentology of Gravels and Conglomerates, Canadian Society of Petroleum Geologists, p. 429-441.

Covault, J. A., Kostic, S., Paull, C. K., Sylvester, Z., and Fildani, A., 2017, Cyclic steps and related supercritical bedforms: Building blocks of deep-water depositional systems, western North America: Mar. Geol., v. 393, p. 4-20.

Cronin, B. T., and Kidd, R. B., 1998, Heterogeneity and lithotype distribution in ancient deep-sea canyons: Point Lobos deep-sea canyon as a reservoir analogue: Sed. Geol., v. 115, no. 1, p. 315-349.

Cunha, M. R., Paterson, G. L. J., Amaro, T., Blackbird, S., de Stigter, H. C., Ferreira, C., Glover, A., Hilário, A., Kiriakoulakis, K., Neal, L., Ravara, A., Rodrigues, C. F., Tiago, Á., and Billett, D. S. M., 2011, Biodiversity of macrofaunal assemblages from three Portuguese submarine canyons (NE Atlantic): Deep Sea Res. Part 2, v. 58, no. 23, p. 2433-2447.

Daly, R. A., 1936, Origin of Submarine Canyons: American Journal of Science, v. 31, no. 186, p. 401-420.

De Leo, F. C., Bernardino, A. F., and Sumida, P. Y. G., 2020, Continental Slope and Submarine Canyons: Benthic Biodiversity and Human Impacts, *in* Sumida, P. Y. G., Bernardino, A. F., and De Léo, F. C., eds., Brazilian Deep-Sea Biodiversity: Cham, Springer International Publishing, p. 37-72.

Deptuck, M. E., Sylvester, Z., Pirmez, C., and O'Byrne, C., 2007, Migration–aggradation history and 3-D seismic geomorphology of submarine channels in the Pleistocene Benin-major Canyon, western Niger Delta slope: Mar. Petrol. Geol., v. 24, no. 6, p. 406-433.

Di Celma, C., Cantalamessa, G., Didaskalou, P., and Lori, P., 2010, Sedimentology, architecture, and sequence stratigraphy of coarse-grained, submarine canyon fills from the Pleistocene (Gelasian-Calabrian) of the Peri-Adriatic basin, central Italy: Mar. Petrol. Geol., v. 27, no. 7, p. 1340-1365.

Dykstra, M., 2012, Deep-Water Tidal Sedimentology, *in* Davis Jr, R. A., and Dalrymple, R. W., eds., Principles of Tidal Sedimentology: Dordrecht, Springer Netherlands, p. 371-395.

Dykstra, M., and Kneller, B., 2009, Lateral accretion in a deep-marine channel complex: implications for channellized flow processes in turbidity currents: Sedimentology, v. 56, no. 5, p. 1411-1432.

Engebretson, D. C., Cox, A., Gordon, R. G., Engebretson, D. C., Cox, A., and Gordon, R. G., 1985, Relative Motions Between Oceanic and Continental Plates in the Pacific Basin, Geological Society of America, 0 p.:

Fildani, A., 2017, Submarine Canyons: A brief review looking forward: Geology, v. 45, no. 4, p. 383-384.

Fildani, A., and Normark, W. R., 2004, Late Quaternary evolution of channel and lobe complexes of Monterey Fan: Mar. Geol., v. 206, no. 1, p. 199-223.

Gallicchio, S., Cerone, D., and Tinterri, R., 2023, Depositional record of confined turbidites in syn-subduction intraslope basin: insight from the Tufiti di Tusa Formation (Southern Apennines, Italy): Mar. Petrol. Geol., v. 147, p. 105969.

Gardner, W. D., 1989, Periodic resuspension in Baltimore canyon by focusing of internal waves: J. Geophys. Res., v. 94, no. C12, p. 18185-18194.

Garrett, C., and Kunze, E., 2007, Internal Tide Generation in the Deep Ocean: Annual Review of Fluid Mechanics, v. 39, no. 1, p. 57-87.

Gastil, R. G., 1975, Reconnaissance geology of the state of Baja California, Boulder, Col, Geological Society of America, Memoir / Geological Society of America ; 140.

Ge, Z., Nemec, W., Gawthorpe, R. L., and Hansen, E. W. M., 2017, Response of unconfined turbidity current to normal-fault topography: Sedimentology, v. 64, no. 4, p. 932-959.

Gladstone, C., McClelland, H. L. O., Woodcock, N. H., Pritchard, D., and Hunt, J. E., 2018, The formation of convolute lamination in mud-rich turbidites: Sedimentology, v. 65, no. 5, p. 1800-1825.

Glazner, A. F., 1991, Plutonism, oblique subduction, and continental growth: An example from the Mesozoic of California: Geology, v. 19, no. 8, p. 784-786.

Hall, R. A., Aslam, T., and Huvenne, V. A. I., 2017, Partly standing internal tides in a dendritic submarine canyon observed by an ocean glider: Deep Sea Res. Part 1, v. 126, p. 73-84.

Hansen, L., Callow, R., Kane, I., and Kneller, B., 2017, Differentiating submarine channel-related thin-bedded turbidite facies: Outcrop examples from the Rosario Formation, Mexico: Sed. Geol., v. 358, p. 19-34.

Hansen, L., Callow, R. H. T., Kane, I. A., Gamberi, F., Rovere, M., Cronin, B. T., and Kneller, B. C., 2015, Genesis and character of thin-bedded turbidites associated with submarine channels: Mar. Petrol. Geol., v. 67, p. 852-879.

Harms, J. C., 1969, Hydraulic significance of some sand ripples: GSA Bulletin, v. 80, no. 3, p. 363-396.

Harris, P. T., Macmillan-Lawler, M., Rupp, J., and Baker, E. K., 2014, Geomorphology of the oceans: Mar. Geol., v. 352, p. 4-24.

Haughton, P. D. W., 1994, Deposits of deflected and ponded turbidity currents, Sorbas Basin, Southeast Spain: J. Sed. Res., v. 64, no. 2a, p. 233-246.

Haughton, P. D. W., Barker, S. P., and McCaffrey, W. D., 2003, 'Linked' debrites in sand-rich turbidite systems – origin and significance: Sedimentology, v. 50, no. 3, p. 459-482.

He, Y.-B., Luo, J.-X., Li, X.-D., Gao, Z.-Z., and Wen, Z., 2011, Evidence of internal-wave and internal-tide deposits in the Middle Ordovician Xujiajuan Formation of the Xiangshan Group, Ningxia, China: Geo-Marine Letters, v. 31, no. 5, p. 509-523.

Heezen, B. C., and Ewing, W. M., 1952, Turbidity currents and submarine slumps, and the 1929 Grand Banks [Newfoundland] earthquake: American Journal of Science, v. 250, p. 849-873.

Hein, F. J., and Walker, R. G., 1982, The Cambro-Ordovician Cap Enragé Formation, Queébec, Canada: conglomeratic deposits of a braided submarine channel with terraces: Sedimentology, v. 29, no. 3, p. 309-352.

Hesse, R., Klaucke, I., Khodabakhsh, S., Piper, D. J. W., Ryan, W. B. F., and Group, N. S., 2001, Sandy Submarine Braid Plains: Potential Deep-Water Reservoirs: AAPG Bulletin, v. 85, no. 8, p. 1499-1521.

Hiscott, R. N., Hall, F. R., and Pirmez, C., 1997, Turbidity-current overspill from the Amazon channel : Texture of the silt/ sand load, paleoflow from anisotropy of magnetic susceptibility and implications for flow processes: Proceedings of the Ocean Drilling Program. Scientific results., v. 155, p. 53-78.

Hiscott, R. N., Middleton, G. V., Doyle, L. J., and Pilkey, O. H., 1979, Depositional Mechanics of Thick-Bedded Sandstones at the Base of a Submarine Slope, Tourelle Formation (Lower Ordovician), Quebec, Canada, Geology of Continental Slopes, 27, SEPM Society for Sedimentary Geology, p. 0.

Hodgson, D. M., Di Celma, C. N., Brunt, R. L., and Flint, S. S., 2011, Submarine slope degradation and aggradation and the stratigraphic evolution of channel–levee systems, v. 168, no. 3, p. 625-628.

Hofstra, M., Peakall, J., Hodgson, D. M., and Stevenson, C. J., 2018, Architecture and morphodynamics of subcritical sediment waves in an ancient channel-lobe transition zone: Sedimentology, v. 65, no. 7, p. 2339-2367.

Ito, M., Ishikawa, K., and Nishida, N., 2014, Distinctive erosional and depositional structures formed at a canyon mouth: A lower Pleistocene deep-water succession in the Kazusa forearc basin on the Boso Peninsula, Japan: Sedimentology, v. 61, no. 7, p. 2042-2062.

Janocko, J., and Basilici, G., 2021, Architecture of coarse-grained gravity flow deposits in a structurally confined submarine canyon (late Eocene Tokaren Conglomerate, Slovakia): Sed. Geol., v. 417, p. 105880.

Jobe, Z. R., Lowe, D. R., and Morris, W. R., 2012, Climbing-ripple successions in turbidite systems: depositional environments, sedimentation rates and accumulation times: Sedimentology, v. 59, no. 3, p. 867-898.

Jobe, Z. R., Sylvester, Z., Parker, A. O., Howes, N., Slowey, N., and Pirmez, C., 2015, Rapid Adjustment of Submarine Channel Architecture To Changes In Sediment Supply: J. Sed. Res., v. 85, no. 6, p. 729-753.

Jopling, A. V., and Walker, R. G., 1968, Morphology and origin of ripple-drift cross-lamination, with examples from the Pleistocene of Massachusetts: J. Sed. Res., v. 38, p. 971-984.

Kane, I. A., Dykstra, M. L., Kneller, B. C., Tremblay, S., and McCaffrey, W. D., 2009, Architecture of a coarse-grained channel–levée system: the Rosario Formation, Baja California, Mexico: Sedimentology, v. 56, no. 7, p. 2207-2234.

Kane, I. A., and Hodgson, D., 2011, Sedimentological criteria to differentiate submarine channel levee subenvironments: exhumed examples from the Rosario Fm. (Upper Cretaceous) of Baja California, Mexico, and the Laingsburg Fm. (Permian), Karoo Basin, S. Africa: Mar. Petrol. Geol., v. 28, p. 807-823.

Kane, I. A., Hodgson, D. M., Hubbard, S. M., McArthur, A. D., Poyatos-Moré, M., Soutter, E. L., Flint, S. S., and Matthews, W., 2022, Deep-water Tectono-Stratigraphy at a Plate Boundary Constrained by Large N-Detrital Zircon and Micropaleontological Approaches: Peninsular Ranges Forearc, Baja California, Mexico: The Sedimentary Record, v. 20, no. 1.

Kane, I. A., Kneller, B. C., Dykstra, M., Kassem, A., and McCaffrey, W. D., 2007, Anatomy of a submarine channel–levee: An example from Upper Cretaceous slope sediments, Rosario Formation, Baja California, Mexico: Mar. Petrol. Geol., v. 24, no. 6-9, p. 540-563.

Keavney, E., Peakall, J., Wang, R., Hodgson, D., Kane, I., Keevil, G., Brown, H., Clare, M., and Hughes, M., 2024, Unconfined gravity current interactions with orthogonal topography: Implications for combined-flow processes and the depositional record: EarthArXiv.

Keevil, G. M., Peakall, J., Best, J. L., and Amos, K. J., 2006, Flow structure in sinuous submarine channels: Velocity and turbulence structure of an experimental submarine channel: Mar. Geol., v. 229, no. 3, p. 241-257.

Kilmer, F. H., 1963, Cretaceous and Cenozoic stratigraphy and palaeontology, El Rosario area.: Berkely, University of California, 149 p p.

Kimbrough, D., Smith, D., Mahoney, J., Moore, T., Grove, M., Gastil, R., Ortega, A., and Fanning, C., 2001, Forearc-basin sedimentary response to rapid Late Cretaceous batholith emplacement in the Peninsular Ranges of southern and Baja California: Geology, v. 29, p. 491-494.

Klaucke, I., and Hesse, R., 1996, Fluvial features in the deep-sea: new insights from the glacigenic submarine drainage system of the Northwest Atlantic Mid-Ocean Channel in the Labrador Sea: Sed. Geol., v. 106, no. 3, p. 223-234.

Kneller, B., 1995, Beyond the turbidite paradigm: physical models for deposition of turbidites and their implications for reservoir prediction: Geol. Soc. London Spec Publ., v. 94, no. 1, p. 31-49.

Kneller, B., 2003, The influence of flow parameters on turbidite slope channel architecture: Mar. Petrol. Geol., v. 20, no. 6, p. 901-910.

Kneller, B., Bozetti, G., Callow, R., Dykstra, M., Hansen, L., Kane, I., Li, P., McArthur, A., Catharina, A. S., Dos Santos, T., and Thompson, P., 2020, Architecture, process, and environmental diversity in a late Cretaceous slope channel system: J. Sed. Res., v. 90, no. 1, p. 1-26.

Kneller, B., and Buckee, C., 2000, The structure and fluid mechanics of turbidity currents: a review of some recent studies and their geological implications: Sedimentology, v. 47, no. s1, p. 62-94.

Kneller, B. C., and Branney, M. J., 1995, Sustained high-density turbidity currents and the deposition of thick massive sands: Sedimentology, v. 42, no. 4, p. 607-616.

Kuenen, P. H., 1966, Experimental Turbidite Lamination in a Circular Flume: J. Geol., v. 74, no. 5, Part 1, p. 523-545.

Lewis, K. B., and Pantin, H. M., 2002, Channel-axis, overbank and drift sediment waves in the southern Hikurangi Trough, New Zealand: Mar. Geol., v. 192, no. 1, p. 123-151.

Li, M. Z., Prescott, R. H., and Robertson, A. G., 2019, Observation of internal tides and sediment transport processes at the head of Logan Canyon on central Scotian Slope, eastern Canada: Journal of Marine Systems, v. 193, p. 103-125.

Li, S., Li, W., Alves, T. M., Wang, J., Feng, Y., Sun, J., Li, J., and Wu, S., 2020, Large-scale scours formed by supercritical turbidity currents along the full length of a submarine canyon, northeast South China Sea: Mar. Geol., v. 424, p. 106158.

Lowe, D., Submarine canyon and slope channel sedimentation model as inferred from Upper Cretaceous deposits, western California, *in* Proceedings 24th International Geological Congress, Montreal, Section1972, Volume 6, p. 75-81.

Lowe, D. R., 1982, Sediment gravity flows; II, Depositional models with special reference to the deposits of high-density turbidity currents: J. Sed. Res., v. 52, no. 1, p. 279-297.

Lowe, D. R., Graham, S. A., Malkowski, M. A., and Das, B., 2019, The role of avulsion and splay development in deep-water channel systems: Sedimentology, architecture, and evolution of the deep-water Pliocene Godavari "A" channel complex, India: Mar. Petrol. Geol., v. 105, p. 81-99.

Lowe, D. R., and Guy, M., 2000, Slurry-flow deposits in the Britannia Formation (Lower Cretaceous), North Sea: a new perspective on the turbidity current and debris flow problem: Sedimentology, v. 47, no. 1, p. 31-70.

Maier, K. L., Fildani, A., McHargue, T. R., Paull, C. K., Graham, S. A., and Caress, D. W., 2012, Punctuated Deep-Water Channel Migration: High-Resolution Subsurface Data from the Lucia Chica Channel System, Offshore California, U.S.A: J. Sed. Res., v. 82, no. 1, p. 1-8.

Maier, K. L., Johnson, S. Y., and Hart, P., 2018, Controls on submarine canyon head evolution: Monterey Canyon, offshore central California: Mar. Geol., v. 404, p. 24-40.

Maier, K. L., Rosenberger, K. J., Paull, C. K., Gwiazda, R., Gales, J., Lorenson, T., Barry, J. P., Talling, P. J., McGann, M., Xu, J., Lundsten, E., Anderson, K., Litvin, S. Y., Parsons, D. R., Clare, M. A., Simmons, S. M., Sumner, E. J., and Cartigny, M. J. B., 2019, Sediment and organic carbon transport and deposition driven by internal tides along Monterey Canyon, offshore California: Deep Sea Res. Part 1, v. 153, p. 103108.

Masson, D. G., Huvenne, V. A. I., de Stigter, H. C., Wolff, G. A., Kiriakoulakis, K., Arzola, R. G., and Blackbird, S., 2010, Efficient burial of carbon in a submarine canyon: Geology, v. 38, no. 9, p. 831-834.

May, J. A., and Warme, J. E., 2007, An Ancient Submarine Canyon, Black's Beach, La Jolla, California, USA, Atlas of Deep-Water Outcrops, AAPG Studies in Geology 56, American Association of Petroleum Geologists.

McArthur, A. D., and McCaffrey, W. D., 2019, Sedimentary architecture of detached deep-marine canyons: Examples from the East Coast Basin of New Zealand: Sedimentology, v. 66, no. 3, p. 1067-1101.

McGee, D. C., 1965, Upper Cretaceous (Campanian) Foraminiferida from Punta Baja, Baja California: AAPG Bulletin, v. 49, no. 7, p. 1087-1087.

Middleton, G. V., and Hampton, M. A., 1973, Sediment gravity flows: mechanics of flow and deposition, *in* Middleton, G. V., and Bouma, A. H., eds., Turbidites and Deep Water Sedimentation: Pacific Section, Short Course, Society of Economic Paleontologists and Mineralogists, p. 1-38.

Millington, J. J., and Clark, J. D., 1995, The Charo/Arro canyon-mouth sheet system, south-central Pyrenees, Spain; a structurally influenced zone of sediment dispersal: J. Sed. Res., v. 65, no. 4b, p. 443-454.

Morris, E. A., 2014, Stratigraphic record of sedimentary processes in submarine channel-levee systems [PhD PhD thesis]: University of Liverpool.

Morris, W., and Busby-Spera, C., 1990, A Submarine-Fan Valley-Levee Complex in the Upper Cretaceous Rosario Formation: Implication for Turbidite Facies Models: Geological Society of America. Geological Society of America Bulletin, v. 102, no. 7, p. 900.

Morris, W. R., and Busby-Spera, C. J., 1988, Sedimentologic Evolution of a Submarine Canyon in a Forearc Basin, Upper Cretaceous Rosario Formation, San Carlos, Mexico: AAPG Bulletin, v. 72, no. 6, p. 717-737.

Mountjoy, J., Howarth, J., Orpin, A., Barnes, P., Bowden, D., Rowden, A., Schimel, A., Holden, C., Horgan, H., Nodder, S., Patton, J., Lamarche, G., Gerstenberger, M., Micallef, A., Pallentin, A., and Kane, T., 2018, Earthquakes drive large-scale submarine canyon development and sediment supply to deep-ocean basins: Science Advances, v. 4, p. eaar3748.

Mutti, E., 1992, Turbidite sandstones, Milan, San Donato, 275 p.:

Nazarian, R. H., Burns, C. M., Legg, S., Buijsman, M. C., Kaur, H., and Arbic, B. K., 2021, On the Magnitude of Canyon-Induced Mixing: Journal of Geophysical Research: Oceans, v. 126, no. 11, p. e2021JC017671.

Normandeau, A., Dafoe, L. T., Li, M. Z., Campbell, D. C., and Jenner, K. A., 2024, Sedimentary record of bottom currents and internal tides in a modern highstand submarine canyon head: Sedimentology, v. n/a, no. n/a.

Patacci, M., Haughton, P. D. W., and Mccaffrey, W. D., 2015, Flow Behavior of Ponded Turbidity Currents: J. Sed. Res., v. 85, no. 8, p. 885-902.

Paull, C. K., Caress, D. W., Lundsten, E., Gwiazda, R., Anderson, K., McGann, M., Conrad, J., Edwards, B., and Sumner, E. J., 2013, Anatomy of the La Jolla Submarine Canyon system; offshore southern California: Mar. Geol., v. 335, p. 16-34.

Paull, C. K., Talling, P. J., Maier, K. L., Parsons, D., Xu, J., Caress, D. W., Gwiazda, R., Lundsten, E. M., Anderson, K., and Barry, J. P. J. N. c., 2018, Powerful turbidity currents driven by dense basal layers, v. 9, no. 1, p. 1-9.

Peakall, J., Best, J., Baas, J. H., Hodgson, D. M., Clare, M. A., Talling, P. J., Dorrell, R. M., and Lee, D. R., 2020, An integrated process-based model of flutes and tool marks in deep-water environments: Implications for palaeohydraulics, the Bouma sequence and hybrid event beds: Sedimentology, v. 67, no. 4, p. 1601-1666.

Peakall, J., McCaffrey, B., and Kneller, B., 2000, A process model for the evolution, morphology, and architecture of sinuous submarine channels: J. Sed. Res., v. 70, no. 3, p. 434-448.

Petruncio, E. T., Rosenfeld, L. K., and Paduan, J. D., 1998, Observations of the Internal Tide in Monterey Canyon: Journal of Physical Oceanography, v. 28, no. 10, p. 1873-1903.

Pickering, K. T., and Corregidor, J., 2005, Mass-Transport Complexes (MTCs) and Tectonic Control on Basin-Floor Submarine Fans, Middle Eocene, South Spanish Pyrenees: J. Sed. Res., v. 75, no. 5, p. 761-783.

Pickering, K. T., and Hiscott, R. N., 1985, Contained (reflected) turbidity currents from the Middle Ordovician Cloridorme Formation, Quebec, Canada: an alternative to the antidune hypothesis: Sedimentology, v. 32, no. 3, p. 373-394.

Piper, D. J. W., and Normark, W. R., 1983, Turbidite depositional patterns and flow characteristics, Navy Submarine Fan, California Borderland: Sedimentology, v. 30, no. 5, p. 681-694.

Pirmez, C., and Imran, J., 2003, Reconstruction of turbidity currents in Amazon Channel: Mar. Petrol. Geol., v. 20, no. 6, p. 823-849.

Privat, A., Peakall, J., Hodgson, D., Schwarz, E., Jackson, C. A. L., and Ariel Arnol, J., 2024, Evolving fill-and-spill patterns across linked early post-rift depocentres control lobe characteristics: Los Molles Formation, Argentina: Sedimentology.

Privat, A. M. L. J., Hodgson, D. M., Jackson, C. A. L., Schwarz, E., and Peakall, J., 2021, Evolution from syn-rift carbonates to early post-rift deep-marine intraslope lobes: The role of rift basin physiography on sedimentation patterns: Sedimentology, v. 68, no. 6, p. 2563-2605.

Puig, P., Palanques, A., and Martín, J., 2014, Contemporary Sediment-Transport Processes in Submarine Canyons: Annual Review of Marine Science, v. 6, no. 1, p. 53-77.

Renne, P. R., Fulford, M. M., and Busby-Spera, C., 1991, High resolution 40AR/39AR chronostratigraphy of the Late Cretaceous El Gallo Formation, Baja California del Norte, Mexico: Geophysical Research Letters, v. 18, no. 3, p. 459-462.

Satur, N., Kelling, G., Cronin, B. T., Hurst, A., and Gürbüz, K., 2005, Sedimentary architecture of a canyon-style fairway feeding a deep-water clastic system, the Miocene Cingöz Formation, southern Turkey: significance for reservoir characterisation and modelling: Sed. Geol., v. 173, no. 1, p. 91-119.

Schwarz, E., and Arnott, R. W. C., 2007, Anatomy and Evolution of a Slope Channel-Complex Set (Neoproterozoic Isaac Formation, Windermere Supergroup, Southern Canadian Cordillera): Implications for Reservoir Characterization: J. Sed. Res., v. 77, no. 2, p. 89-109.

Shanmugam, G., 2003, Deep-marine tidal bottom currents and their reworked sands in modern and ancient submarine canyons: Mar. Petrol. Geol., v. 20, no. 5, p. 471-491.

Shanmugam, G., and Wang, Y., 2014, Review of research in internal-wave and internal-tide deposits of China: Discussion: Journal of Palaeogeography, v. 3, no. 4, p. 332-350.

Shepard, F. P., 1972, Submarine canyons: Earth-Sci. Rev., v. 8, no. 1, p. 1-12.

Shepard, F. P., 1976, Tidal Components of Currents in Submarine Canyons: J. Geol., v. 84, no. 3, p. 343-350.

Shepard, F. P., and Marshall, N. F., 1969, Currents in La Jolla and Scripps Submarine Canyons: Science, v. 165, no. 3889, p. 177-178.

Shepard, F. P., Marshall, N. F., McLoughlin, P. A., Sullivan, G. G., Shepard, F. P., Marshall, N. F., McLoughlin, P. A., and Sullivan, G. G., 1979, Currents in Submarine Canyons and Other Seavalleys, Currents in Submarine Canyons and Other Seavalleys, 8, American Association of Petroleum Geologists, p. 0.

Sohn, Y. K., 1997, On traction-carpet sedimentation: J. Sed. Res., v. 67, no. 3, p. 502-509.

Soutter, E., Kane, I., Hunt, J. E., Huvenne, V. A. I., Charidemou, M., Garnett, R., Edwards, M., Bett, B., Mienis, F., Hall, R., Gates, A., Wolfe, M., and Clare, M. A., 2024, Interactions between internal tides and turbidity currents: an under-recognized process in deep-marine stratigraphy?: ESE Open Archive.

Soutter, E. L., Bell, D., Cumberpatch, Z. A., Ferguson, R. A., Spychala, Y. T., Kane, I. A., and Eggenhuisen, J. T., 2021, The Influence of Confining Topography Orientation on Experimental Turbidity Currents and Geological Implications: Front. Earth Sci., v. 8.

Stanley, D. J., Submarine canyon and slope sedimentation (Grès d'Annot) in the French Maritime Alps, *in* Proceedings 9th International Congress of Sedimentology, Nice, 1975 1975, p. 129.

Stevenson, C. J., Jackson, C. A.-L., Hodgson, D. M., Hubbard, S. M., and Eggenhuisen, J. T., 2015, Deep-Water Sediment Bypass: J. Sed. Res., v. 85, no. 9, p. 1058-1081.

Stevenson, C. J., Peakall, J., Hodgson, D. M., Bell, D., and Privat, A., 2020, T_B or not T_B: banding in turbidite sandstones: J. Sed. Res., v. 90, no. 8, p. 821-842.

Stevenson, C. J., Talling, P. J., Wynn, R. B., Masson, D. G., Hunt, J. E., Frenz, M., Akhmetzhanhov, A., and Cronin, B. T., 2013, The flows that left no trace: Very large-volume turbidity currents that bypassed sediment through submarine channels without eroding the sea floor: Mar. Petrol. Geol., v. 41, p. 186-205.

Stow, D., and Johansson, M., 2000, Deep-water massive sands: Nature, origin and hydrocarbon implications: Mar. Petrol. Geol., v. 17, p. 145-174.

Sumner, E. J., Amy, L. A., and Talling, P. J., 2008, Deposit Structure and Processes of Sand Deposition from Decelerating Sediment Suspensions: J. Sed. Res., v. 78, no. 8, p. 529-547.

Sumner, E. J., Talling, P. J., and Amy, L. A., 2009, Deposits of flows transitional between turbidity current and debris flow: Geology, v. 37, no. 11, p. 991-994.

Sweet, M. L., Marsset, T., Toucanne, S., Rittenour, T. M., Jouet, G., Gaillot, G. T., and Blum, M. D., 2019, Sediment routing from shelf to basin floor in the Quaternary Golo System of Eastern Corsica, France, western Mediterranean Sea: GSA Bulletin, v. 132, no. 5-6, p. 1217-1234.

Symons, W. O., Sumner, E. J., Talling, P. J., Cartigny, M. J. B., and Clare, M. A., 2016, Large-scale sediment waves and scours on the modern seafloor and their implications for the prevalence of supercritical flows: Mar. Geol., v. 371, no. C, p. 130-148.

Talling, P. J., Amy, L. A., Wynn, R. B., Peakall, J., and Robinson, M., 2004, Beds comprising debrite sandwiched within co-genetic turbidite: origin and widespread occurrence in distal depositional environments: Sedimentology, v. 51, no. 1, p. 163-194.

Talling, P. J., Baker, M. L., Pope, E. L., Ruffell, S. C., Jacinto, R. S., Heijnen, M. S., Hage, S., Simmons, S. M., Hasenhündl, M., Heerema, C. J., McGhee, C., Apprioual, R., Ferrant, A., Cartigny, M. J. B., Parsons, D. R., Clare, M. A., Tshimanga, R. M., Trigg, M. A., Cula, C. A., Faria, R., Gaillot, A., Bola, G., Wallance, D., Griffiths, A., Nunny, R., Urlaub, M., Peirce, C., Burnett, R., Neasham, J., and Hilton, R. J., 2022, Longest sediment flows yet measured show how major rivers connect efficiently to deep sea: Nat. Commun., v. 13, no. 1, p. 4193.

Talling, P. J., Cartigny, M. J. B., Pope, E., Baker, M., Clare, M. A., Heijnen, M., Hage, S., Parsons, D. R., Simmons, S. M., Paull, C. K., Gwiazda, R., Lintern, G., Hughes Clarke, J. E., Xu, J., Silva Jacinto, R., and Maier, K. L., 2023, Detailed monitoring reveals the nature of submarine turbidity currents: Nature Reviews Earth & Environment, v. 4, no. 9, p. 642-658.

Talling, P. J., Masson, D. G., Sumner, E. J., and Malgesini, G., 2012, Subaqueous sediment density flows: Depositional processes and deposit types: Sedimentology, v. 59, no. 7, p. 1937-2003.

Taylor, W. J., Hodgson, D. M., Peakall, J., Kane, I. A., Morris, E. A., and Flint, S. S., 2024, Unidirectional and combined transitional flow bedforms: Controls on process and distribution in submarine slope settings: Sedimentology.

Tek, D. E., McArthur, A. D., Poyatos-Moré, M., Colombera, L., Patacci, M., Craven, B., and McCaffrey, W. D., 2021, Relating seafloor geomorphology to subsurface architecture: How mass-transport deposits and knickpoint-zones build the stratigraphy of the deep-water Hikurangi Channel: Sedimentology, v. 68, no. 7, p. 3141-3190.

Tinterri, R., 2011, Combined flow sedimentary structures and the genetic link between sigmoidal- and hummocky-cross stratification: GeoActa, v. 10, p. 43-85.

Tinterri, R., Mazza, T., and Magalhaes, P. M., 2022, Contained-Reflected Megaturbidites of the Marnoso-arenacea Formation (Contessa Key Bed) and Helminthoid Flysches (Northern Apennines, Italy) and Hecho Group (South-Western Pyrenees): Front. Earth Sci., v. 10, p. 817012.

Tubau, X., Paull, C. K., Lastras, G., Caress, D. W., Canals, M., Lundsten, E., Anderson, K., Gwiazda, R., and Amblas, D., 2015, Submarine canyons of Santa Monica Bay, Southern California: Variability in morphology and sedimentary processes: Mar. Geol., v. 365, p. 61-79.

van Haren, H., Mienis, F., and Duineveld, G., 2022, Contrasting internal tide turbulence in a tributary of the Whittard Canyon: Continental Shelf Research, v. 236, p. 104679.

von Rad, U., and Tahir, M., 1997, Late Quaternary sedimentation on the outer Indus shelf and slope (Pakistan): evidence from high-resolution seismic data and coring: Mar. Geol., v. 138, no. 3, p. 193-236.

Wain, D. J., Gregg, M. C., Alford, M. H., Lien, R.-C., Hall, R. A., and Carter, G. S., 2013, Propagation and dissipation of the internal tide in upper Monterey Canyon: Journal of Geophysical Research: Oceans, v. 118, no. 10, p. 4855-4877.

Wang, Z., and Plate, E. C. H. J., 1996, A preliminary study on the turbulence structure of flows of non-Newtonian fluid: J. Hydraul. Res., v. 34, no. 3, p. 345-361.

Winterwerp, J. C., and van Kesteren, W. G. M., 2004, Flocculation Processes, *in* Winterwerp, J. C., and van Kesteren, W. G. M., eds., Introduction to the Physics of Cohesive Sediment in the Marine Environment, 56: Amsterdam, Elsevier, p. 87-119.

Wynn, R. B., Cronin, B. T., and Peakall, J., 2007, Sinuous deep-water channels: Genesis, geometry and architecture: Mar. Petrol. Geol., v. 24, no. 6, p. 341-387.

Wynn, R. B., Piper, D. J. W., and Gee, M. J. R., 2002, Generation and migration of coarse-grained sediment waves in turbidity current channels and channel–lobe transition zones: Mar. Geol., v. 192, no. 1, p. 59-78.

Yang, Y., Maselli, V., Normandeau, A., Piper, D. J. W., Li, M. Z., Campbell, D. C., Gregory, T., and Gao, S., 2020, Latitudinal Response of Storm Activity to Abrupt Climate Change During the Last 6,500 Years: Geophysical Research Letters, v. 47, no. 19, p. e2020GL089859.

Zhenzhong, G., and Eriksson, K. A., 1991, Internal-tide deposits in an Ordovician submarine channel: Previously unrecognized facies?: Geology, v. 19, no. 7, p. 734-737.

Zhong, G., and Peng, X., 2021, Transport and accumulation of plastic litter in submarine canyons—The role of gravity flows: Geology, v. 49, no. 5, p. 581-586.

Zhu, M., Graham, S., Pang, X., and McHargue, T., 2010, Characteristics of migrating submarine canyons from the middle Miocene to present: Implications for paleoceanographic circulation, northern South China Sea: Mar. Petrol. Geol., v. 27, no. 1, p. 307-319.

LIST OF FIGURES

Figure 1. (A) Geological map of part of the Baja California peninsula, showing the main units of the Peninsular Ranges forearc basin complex. Modified from Morris and Busby-Spera (1990) and Kneller et al. (2020). (B) Stratigraphic column showing the main formations and depositional settings of the Peninsular Ranges forearc basin complex.

Figure 2. (A) Zoomed-in geological map of the Punta Baja overbank (location shown in B). (B) Geological map of the Punta Baja peninsula, with the main formations and facies associations within the Punta Baja Formation overlain onto a drone-captured digital elevation model (DEM). Map location is shown in Figure 5.1. (C) Equal-area rose diagrams showing palaeocurrent directions from conglomerate clast imbrication, flute, groove and ripple foresets for each of the main facies associations.

Figure 3. Schematic cross section of the Punta Baja canyon-fill, with photographs highlighting the main facies associations. (A) Overbank packages onlapping onto the Bocana Roja Fm. (B) Canyon axis packages overlying MTDs and channel margin packages. (C) Channel margin packages thinning and onlapping onto steep erosion surfaces. (D) Shallow marine packages truncated by the El Gallo unconformity. (E) Overbank packages within the upper overbank. (F) Overbank packages onlapping onto the Bocana Roja Fm. that are truncated by the overlying El Gallo unconformity. (G) Scour-fill and prominent sandstone bar forms in the canyon axis. (H) Channel margin sandstone packages interbedded with axial conglomerates.

Figure 4. Sketch bed diagrams and representative outcrop photographs which highlight the internal divisions of: (A) HDT 1 beds; (B) HDT 2 beds; (C) LDT 1 beds; (D) LDT 2 beds; (E) TFD 1 beds; (F) TFD 2 beds; (G) TFD 3 beds; and (H) ITDs. HDT, high-density turbidite; LDT, low-density turbidite; TFD, transitional flow deposit; ITD, internal tide deposit; SCRs, sand-rich current ripples; BRs,

biconvex ripples; LABWs, low-amplitude bed-waves; MCRs, mud-rich current ripples; LBRs, large biconvex ripples; HLCS, hummock-like cross stratification.

Figure 5. Graph showing the average wavelengths and amplitudes of different bedform types observed within turbulent and transitional flow beds throughout the Punta Baja overbank. Bedform amplitude is plotted with a logarithmic scale.

Figure 6. (A) Boxen plot showing the distribution of sandstone and mudstone beds from the upper and lower overbank. (B) Violin plot showing the grain-size distribution of sandstone beds from the upper and lower overbank. (C) Bar plot showing the proportions of the different bed types by total measured stratigraphic thickness of the upper and lower overbank. Proximal refers to locations close to channel-fills, whilst distal refers to locations near the canyon margin. HDT, high-density turbidite; LDT, low-density turbidite; TFD, transitional flow deposit; ITD, internal tide deposit; MTD, mass-transport deposit.

Figure 7. Composite log, bed type proportions and representative photographs through the lower overbank section (Stage 1). (A) LDT 2 beds with structureless and biconvex ripple divisions. (B) Structureless LDT 1 bed which passes into sandy starved ripples. (C) HDT 1 bed thickening into an MTD. (D) Overturned bedding against an MTD at the canyon margin. (E) LDT 2 beds containing sand-rich biconvex ripples. HDT, high-density turbidite; LDT, low-density turbidite; TFD, transitional flow deposit; ITD, internal tide deposit; MTD, mass-transport deposit.

Figure 8. (A) UAV-captured photogrammetric model of channel margin, lower and upper overbank packages of the Punta Baja canyon-fill, with sedimentary logs projected onto the model. (B) Correlation panel of the margin and overbank packages, with drawn interpretations of the constituent beds, highlighting their lateral and stratigraphic variability. (C) Photograph of medium- to thick-bedded sandstone packages interpreted as a channel margin deposit. (D) Photograph of the confined overbank showing the differences in bed thickness and grain-size between the lower and upper overbank stages. Panel location is shown in Figure 2B. Rose diagrams are oriented with respect to the panel.

Figure 9. (A) UAV-captured photogrammetric model of the lower and upper overbank packages of the Punta Baja Formation near the canyon margin, with sedimentary logs projected onto the model. (B) Correlation panel of the overbank section, with drawn interpretations of the main package types, highlighting the lateral and stratigraphic variability of their constituent beds and their interactions with the canyon wall. (C) Photograph of upper overbank packages onlapping onto the canyon wall (Bocana Roja Fm.) and planed off by the overlying El Gallo Fm. (D) Photograph of beds within the lower overbank packages. Beds have been overturned with proximity to MTDs, which were caused by canyon margin failure. (E) Photograph of lower overbank thin-bedded packages which have been rotated due to lateral migration of the channel axis. Location of the panel is shown in Figure 2B. Rose diagrams are orientated with respect to the panel.

Figure 10. Composite log, bed type proportions and representative photographs through the upper overbank section (Stage 2). (A) TFD 3 bed containing LABWs overlain by a TFD 1 bed containing mud-rich current ripples. (B) TFD 1 beds comprising a basal division of mud-rich current ripples before passing into a division of longer, thinner low-amplitude bed-waves and starved ripples. (C) TFD 1 beds with large mud-rich ripples. (D) ITD bed showing reworking of a (sand-rich) sediment gravity flow deposit by internal tides, characterised by 'rhythmic' thin-thick lamination and starved ripples. (E) TFD 2 beds, demonstrating sandstone-mudstone banded sets and mud-rich ripples. HDT, high-density turbidite; LDT, low-density turbidite; TFD, transitional flow deposit; ITD, internal tide deposit; MTD, mass-transport deposit; LABW, low-amplitude bed-wave.

Figure 11. Bed-scale correlation panel of a representative 2-metre section from the upper overbank highlighting the across-strike distribution and lateral transitions of the different bed types over a distance of 100-200 metres. HDT, high-density turbidite; LDT, low-density turbidite; TFD, transitional flow deposit; ITD, internal tide deposit; MTD, mass-transport deposit.

Figure 12. Conceptual diagram of a canyon setting, showing the locations where different flow transformations and bed types are expected to form. (A) Lower overbank stage where high-magnitude, erosional flows are the dominant process. (B) Lower overbank stage where lower magnitude flows are affected by complex canyon topography. (C) Upper overbank stage, where canyon widening creates

sufficient accommodation for flow to overspill and transform between turbulent and laminar states. HDT, high-density turbidite; LDT, low-density turbidite; TFD, transitional flow deposit; ITD, internal tide deposit.

LIST OF TABLES